2015-11-01

The Anatomy of Porcine and Human Larynges: Structural Analysis and High Resolution Magnetic Resonance Imaging of the Recurrent Laryngeal Nerve

Nena Lundgreen Mason
Brigham Young University - Provo

The Anatomy of Porcine and Human Larynges: Structural Analysis

and High Resolution Magnetic Resonance Imaging of the

Recurrent Laryngeal Nerve

Nena Lundgreen Mason

A dissertation submitted to the faculty of
Brigham Young University
in partial fulfillment of the requirements for the degree of

Doctor of Philosophy

Jonathan J. Wisco, Chair
Michael D. Brown
Sterling N. Sudweeks
Kristine M. Tanner
Neal K. Bangerter

Department of Physiology and Developmental Biology

Brigham Young University

December 2015

ABSTRACT

The Anatomy of Porcine and Human Larynges: Structural Analysis
and High Resolution Magnetic Resonance Imaging of the
Recurrent Laryngeal Nerve

Nena Lundgreen Mason
Department of Physiology and Developmental Biology, BYU
Doctor of Philosophy

The recurrent laryngeal nerve (RLN) innervates all the intrinsic muscles of the larynx that are responsible for human vocalization and language. The RLN runs along the tracheoesophageal groove bilaterally and is often accidentally damaged or transected during head and neck surgical procedures. RLN palsy and vocal cord paralysis are the most common and serious post op complications of thyroid surgeries. Patients who suffer from RLN injury can develop unilateral or bilateral vocal fold paralysis (BVFP). Theoretically, selective reinnervation of the posterior cricoarytenoid muscle would be the best treatment for BVFP. The phrenic nerve has been shown in several studies to be the best candidate to anastomose to the distal end of a severed RLN to restore glottal abduction. Successful PCA reinnervation has been sporadically achieved in both human patients and in animal models. Another notable ramification of recurrent laryngeal nerve injury is vocal instability caused by the alteration of mechanical properties within the larynx. In phonosurgery, alterations to the position and framework of the laryngeal apparatus are made to improve voice quality. Accurate and realistic synthetic models are greatly needed to predict the outcome of various adjustments to vocal cord tension and position that could be made surgically. Despite the sporadically successful attempts at PCA reinnervation, thus far, there are still several deficits in our anatomical familiarity and technological capability, which hinder the regularity of successful PCA reinnervation surgeries and our capacity to generate synthetic models of the human larynx that are both realistic and functional. We will address three of these deficits in this project using the porcine larynx as a model. Firstly, we will identify the anatomical variations of the porcine recurrent laryngeal nerve branches. A microscribe digitizer will be used to create three-dimensional mapping of the recurrent laryngeal nerve branches that are relevant to the posterior cricoarytenoid muscle and the abduction of the vocal folds. Secondly, we will develop a magnetic resonance imaging technique to correlate recurrent laryngeal nerve branching patterns with high-resolution MR images that can be used to determine the branching patterns present in a given specimen without surgery. Lastly, we will determine the distribution and composition of different tissue types found within human vocal folds. High resolution MRI, and Mallory's trichrome and H&E histological staining will be used to distinguish and identify the tissue composition of the vocal folds and surrounding laryngeal structures. Detailed information regarding vocal fold tissue composition and histological geometry will enable laryngeal modelers to select more sophisticated and life-like materials with which to construct synthetic vocal fold models.

ACKNOWLEDGMENTS

I am immensely grateful for the constant support and guidance that my mentor, Dr. Jonathan Wisco, offered me throughout these research projects. I will always be very grateful for his monumental efforts on my behalf. Dr. Wisco helped me to develop my own talents and gave me a wonderful example of what a kind, supportive, and patient mentor should be like. I am also thankful for the efforts and advice of the members of my graduate committee, Drs. Michael Brown, Sterling Sudweeks, Kristine Tanner, and Neal Bangerter.

I would like to thank my family, especially my wonderful parents, who have made my education possible and never had anything but relentless support and love to offer me as I struggled through both my undergraduate and graduate education.

I would also like to give special mention to Dr. Jason Shaw who convinced me as a young student to be brave and aspire to much more than I ever would have on my own. It is a remarkable and rare teacher that can inspire a student to reach so high when they themselves have little faith in their own capabilities. I absolutely would not be here without your confidence in me, your encouragement, and your kindness. I someday hope to become the type of educator that can inspire and lift students in the same way that you did for me.

TABLE OF CONTENTS

LIST OF FIGURES

CHAPTER 1: Introduction

The vocal cords are folds of tough mucus membrane situated within the larynx. The movements of the vocal folds are responsible for several important physiologic functions. The abduction and adduction of the vocal folds open and close off the flow of air through the trachea to the lungs. The full adduction of the vocal folds closes off the tracheal opening and helps prevents aspiration during swallowing, and abduction of the vocal folds opens the trachea and allows for deep respirations. The numerous and complex sounds of human vocalization and language production are created by the oscillation of the vocal folds. Vocal fold movement is facilitated by a series of muscles that surround the larynx. Abduction is carried out by the posterior cricoarytenoid muscle (PCA), and adduction is facilitated by several synergistic intrinsic muscles of the larynx.

Bilateral vocal fold paralysis (BVFP), or the immobilization of both vocal cords, is a condition that can be caused by compromise of the bilateral recurrent laryngeal nerves (RLN) or the laryngeal muscles that manipulate the voice box. The RLN is often transected or otherwise damaged during neck surgery. Damage to the RLN or the laryngeal muscle can be also be caused by head and neck injuries, tumors, disease, or stroke. According to the American Academy of Otolaryngology-Head and Neck Surgery, without the innervation of the RLN, the function of the vocal folds is lost and patients are subject to respiratory compromise, aspiration, and loss of phonation.

Theoretically, selective reinnervation of the PCA muscle would be the best treatment for BVFP. The phrenic nerve has been shown in several studies to be the best candidate to anastomose to the distal end of a severed RLN. The phrenic nerve has been shown to be compatible in histological, electrophysiological, and anatomical studies for reinnervation of the

PCA [1, 2] The Phrenic nerve has been used in several animal studies to reinnervate the PCA muscle and successfully re-establish vocal fold abduction [2, 3]. Success with this surgical technique has been sporadically achieved in human and animal models throughout the literature [2-4] Despite the successful attempts at PCA reinnervation, thus far, there are still several deficits in our anatomical familiarity and technological capability, which hinder the regularity of successful recurrent laryngeal/phrenic nerve reinnervation surgeries, three of which we will address in this proposal using the porcine larynx as a model.

We have framed our specific aims and experiments to address the following three gaps in our current knowledge of the porcine and human laryngeal anatomy. The first gap, which is addressed by Specific aim 1, is a lack of modern three-dimensional mapping of the RLN showing all the anatomical variations. Accurate mapping is essential to good surgical planning. The RLN mapping that is currently available is crude, rudimentary, and does not provide adequate information regarding nerve location, variation, and dimension. Secondly, addressed in Specific Aim 2, there is a great need for a diagnostic imaging method that can be used to determine which anatomical variation of the RLN is present in a particular patient without exploratory surgery. Many patients with BVFP undergo exploratory surgery to determine if they are candidates for a PCA reinnervation procedure only to discover they don't have the indicated RLN anatomy for surgical anastomosis.

The third gap addressed in Specific Aim 3 involves determining the 3D histological and geometric structure of the human larynx. We propose to determine the distribution and composition of different tissue types found within and around the human vocal folds. High resolution MR images of porcine vocal folds will be obtained to view tissue composition and variation throughout the vocal folds via image contrast. A Mallory's trichrome histological stain

will also be used to locate all cartilaginous structures and view their configuration within the vocal folds. H&E histological staining will also be used to distinguish and identify the tissue composition of the vocal folds. When analyzed together the histological images and MR images will yield a 3D understanding of vocal fold tissue composition.

Research Strategy and Specific Aims

Specific Aim 1:

We will identify the anatomical variations of the porcine recurrent laryngeal nerve branches. A MicroScribe digitizer will be used to create three-dimensional mapping of the recurrent laryngeal nerve branches that are relevant to the posterior cricoarytenoid muscle and the abduction of the vocal folds.

The branching patterns of the phrenic nerve and RLN are variable and complex [5, 6]. Two dimensional schematics and crude drawings have been published that illustrate the general branching patterns of human and animal laryngeal and phrenic nerves. [6-8] Knight et al. Another study specifically provided the general pathway of the porcine RLN and the pathways taken by the abductor branch to the PCA using Sihler's stain [9]. However they did not provide any information about anatomical variation of porcine RLN branching patterns, nor did they show where the other RLN branches, which innervate the adductor muscles, run within the larynx. We present preliminary data (figure 2.1) that shows the anatomical variations of porcine RLN branching patterns in dissected specimens, and the percent of occurrence of each pattern. This data will serve as a valuable first step in producing (3D) models of the RLN and its branching patterns. 3D mapping of nerve pathways would enable surgeons to decrease the likelihood of unintentional RLN transection during head and neck surgical procedures by providing them with more accurate representations of nerve pathways that would include

valuable information regarding nerve location, variation, and dimension. 3D mapping of the RLN would also reveal the best location to ligate and anastomose the RLN and phrenic nerves prior to surgery, while decreasing the likelihood of laryngeal synkinesis during reinnervation surgeries by clarifying where exactly the branches are located in three dimensions.

Specific Aim 2:

We will develop a magnetic resonance imaging (MRI) technique to correlate recurrent laryngeal nerve branching patterns with high-resolution MRI images that can be used to determine the branching patterns present in a given specimen without surgery.

A second major deficiency with current BVFP treatment procedures is that the anatomical nerve variation of a particular patient is unknown before surgery. There are many different procedures for RLN/phrenic nerve anastomosis which are listed by Meng Li et al. in their 2013 publication [1]. The best surgical plan to be used for a particular BVFP patient depends on the anatomical variation present in that patient. Determining candidacy for a particular procedure without surgery is currently not possible. If a method can be developed to use high resolution MRI images of the larynx to determine which branching pattern a patient has pre-op, more accurate and efficient surgical plans can be made in advance and surgical candidacy can be determined without invasive exploratory surgery.

Porcine anatomy is very similar to that found in humans. [10, 11] If a diagnostic technique can be developed to use MR imaging to determine which branching pattern is present in a pig specimen it may be possible to perform a similar method with human patients. Human RLN branching patterns have been well studied [5, 6, 7, 12]. We propose to correlate branching patterns discovered by dissection with high resolution MRI imaging of our porcine larynges to identify which branching pattern is present in a particular specimen. This new MRI technique

4

will serve as in important stepping stone to determining surgical candidacy in humans in a non-invasive manner.

Specific Aim 3:

We will determine the distribution and composition of the different tissue types found within the human vocal folds and surrounding laryngeal tissue. High resolution MR images of human vocal folds will be obtained to view tissue composition and variation throughout the vocal folds via image contrast. High resolution MR images will be analyzed alongside H&E and Mallory's trichrome histological staining to correlate tissue contrast with specific cell type.

One ramification of RLN injury is vocal instability caused by the alteration of mechanical properties within the larynx.[13] In phonosurgery, alterations to the position and framework of the laryngeal apparatus are made to improve voice quality. Accurate and realistic synthetic models are greatly needed to predict the outcome of various adjustments to vocal cord tension and position that could be made surgically. Laryngeal models that are currently in use are all based on the pig model. We propose to determine the distribution and composition of different tissue types found within porcine vocal folds. High resolution MRI, and Mallory's trichrome and H&E histological staining will be used to distinguish and identify the tissue composition of the vocal folds. Detailed information regarding vocal fold tissue composition and histological geometry will enable laryngeal modelers to select more sophisticated and life-like materials with which to construct synthetic vocal fold models.

References

1. Li, Meng, et al. "Reinnervation of Bilateral Posterior Cricoarytenoid Muscles Using the Left Phrenic Nerve in Patients with Bilateral Vocal Fold Paralysis."PloS one 8.10 (2013): e77233.

2. Crumley, R. L. "Phrenic nerve graft for bilateral vocal cord paralysis." The Laryngoscope 93.4 (1983): 425-428.

3. van Lith-Bijl, Julie T., et al. "Laryngeal abductor reinnervation with a phrenic nerve transfer after a 9-month delay." Archives of Otolaryngology–Head & Neck Surgery 124.4 (1998): 393-398.

4. Jacobs, I. N., et al. "Reinnervation of the canine posterior cricoarytenoid muscle with sympathetic preganglionic neurons." The Annals of otology, rhinology, and laryngology 99.3 Pt 1 (1990): 167-174.

5. Maranillo, Eva, et al. "Variability of the nerve supply patterns of the human posterior cricoarytenoid muscle." The Laryngoscope 113.4 (2003): 602-606.

6. Sanders, Ira, et al. "The innervation of the human larynx." Archives of Otolaryngology–Head & Neck Surgery 119.9 (1993): 934-939.

7. Damrose, Edward J., et al. "Surgical anatomy of the recurrent laryngeal nerve: implications for laryngeal reinnervation." The Annals of otology, rhinology, and laryngology 112.5 (2003): 434-438.

8. Mendelsohn, Abie H., et al. "Cervical variations of the phrenic nerve." The Laryngoscope 121.9 (2011): 1920-1923.

9. Knight, Melanie J., Stephen E. McDonald, and Martin A. Birchall. "Intrinsic muscles and distribution of the recurrent laryngeal nerve in the pig larynx."European Archives of Oto-Rhino-Laryngology and Head & Neck 262.4 (2005): 281-285.

10. Stavroulaki, P., and M. Birchall. "Comparative study of the laryngeal innervation in humans and animals employed in laryngeal transplantation research." The Journal of Laryngology & Otology 115.04 (2001): 257-266.

11. Jiang, JACK J., JOSEPH R. Raviv, and DAVID G. Hanson. "Comparison of the phonation-related structures among pig, dog, white-tailed deer, and human larynges." ANNALS OF OTOLOGY RHINOLOGY AND LARYNGOLOGY110.12 (2001): 1120-1125.

12. Ardito, Guglielmo, et al. "Revisited anatomy of the recurrent laryngeal nerves."The American journal of surgery 187.2 (2004): 249-253.

13. Min, Young B., Ingo R. Titze, and Fariborz Alipour-Haghighi. "Stress-strain response of the human vocal ligament." Annals of Otology, Rhinology & Laryngology 104.7 (1995): 563-569.

CHAPTER 2: 3D Reconstruction and Heat Map of Porcine Recurrent Laryngeal Nerve
Anatomy: Branching and Spatial Location

Authors:
Nena Lundgreen Mason[1], Marc Christiansen[1], Jonathan J. Wisco, Ph.D.[1,2]

Affiliations:
[1]Department of Physiology and Developmental Biology, Neuroscience Center, Brigham Young University, Provo, UT
[2]Department of Neurobiology and Anatomy, University of Utah Medical School, Salt Lake City, UT

Corresponding Author:

Nena Lundgreen Mason

Department of Physiology and Developmental Biology
Brigham Young University
Laboratory for Translational Anatomy of Degenerative Diseases and Developmental Disorders
4005 LSB Provo, UT 84602-1231

Phone: 208-249-0558
Fax: 801-422-0004
Email: nenalundgreen@gmail.com

Abstract

Recurrent laryngeal nerve (RLN) palsy is a common post-operative complication of many head and neck surgeries.[1] The best treatment to restore partial function to a damaged RLN is reinnervation of the posterior cricoarytenoid (PCA) muscle via anastomosis of the RLN and phrenic nerves. The pig is an excellent model of human laryngeal anatomy and physiology.[2] A thorough knowledge of porcine laryngeal anatomy is necessary before the pig can be used to improve existing surgical strategies, and develop new ones. This study first identifies the three most common RLN branching patterns in the pig. Secondly, this study presents state of the art three dimensional renderings of the porcine larynx which accurately display the structure and location of the RLN within the larynx. Lastly, several heat maps are also presented that describe the relative spatial variability of 32 bilateral specimens of the RLN trunks and primary branches respectively. We intend this study to be useful to groups using a porcine model to study PCA reinnervation techniques.

Introduction

Vocal cord paralysis is a common post-operative complication of head and neck procedures that is caused by damage to the recurrent laryngeal nerve (RLN).[1] Vocal cord paralysis can cause respiratory compromise if innervation to the posterior cricoarytenoid muscle (PCA) is compromised. PCA compromise renders the vocal folds unable to abduct, yielding respiratory compromise. In theory, the most effective way to correct this problem would be to selectively reinnervate the PCA. Reinnervation of the PCA has been achieved via anastomosis of the RLN with the phrenic nerve in both human and animal models.[3-6] The phrenic nerve is the best choice for anastomosis with the RLN because the two nerves are compatible in histological, electrophysiological, and anatomical parameters.[3-6] Because phrenic/RLN anastomosis is the

best treatment for vocal cord paralysis but current methods are not consistently successful improvements need to be made to this surgical strategy.

Animal models have long been used to develop and improve surgical strategies for use on human patients. Ideal animal model selection for surgical development is generally dependent on the how analogous a particular animal is to human anatomy. The pig larynx has the most analogous anatomy to that of humans. Pigs have been shown to possess the most similar laryngeal anatomy[7], neuroanatomy[8], mucosal histology[7], and phonatory characteristics[2, 9] to the human larynx of all the various animal models that have been used in past studies. Due to these many similarities between human and porcine laryngeal anatomy the pig is the ideal choice to employ in the development and improvement of PCA reinnervation surgical procedures. As with any surgery a detailed understanding of the anatomy and possible anatomical structural variation involved is necessary. Because the pig is the ideal model for PCA reinnervation surgeries we must comprehend all the anatomical details of the porcine larynx so that effective pre-clinical studies can be developed using the pig model.

Traditional anatomy atlases contain detailed 2D drawings of body structures. A two dimensional atlas does not include vital information that well planned surgeries require such as, depth of a particular structure, precise distance from surrounding structures, and spatial relationships between different tissue types. 3D anatomical representations of body structures reflect true anatomical arrangement and eliminate the risk of misrepresentation of 3D structures which is common amongst 2D diagrams. Currently this type of spatial information is available through dissection experience, exploratory surgery and a few imaging techniques. Various techniques exist to obtain images of anatomical structures that are accurate in three dimensions such as volume rendering[10, 11], but these techniques require expensive CT equipment and are

only available to those with access to medical facilities. Surgical planning, anatomical education, and preclinical research would be greatly improved by access to accurate 3D representations of anatomical structures. In this study we present 3D models of the porcine recurrent laryngeal nerve to be used for educational anatomical instruction, and planning for PCA reinnervation surgical experimentation. Each nerve is shown in accurate relation to surrounding laryngeal structures including the thyroid and arytenoid cartilages, posterior cricoarytenoid muscle, epiglottis, and trachea. This study is intended to be useful to groups using the pig to develop new PCA reinnervation surgical strategies and improve existing ones.

Materials and Methods

Animals

Porcine larynges used in this study were donated by Circle V Meats (Spanish Fork, Utah). Larynx specimens were opportunity samples obtained from animals that were sacrificed for commercial purposes. 34 cadaveric larynges were dissected to obtain detailed 3D maps of 32 RLNs. Excess tissue was removed from each specimen leaving only cartilage, trachea, esophagus, laryngeal nerves, and intrinsic muscles of the larynx. A 10% formalin solution was used to fix and preserve the larynges after a postmortem time of 1 hour.

Anatomical Variation of the Porcine Recurrent Laryngeal Nerve

Twenty-eight RLN's were exposed in 15 embalmed bilateral larynx specimens. One of our larynx specimens was damaged bilaterally during dissection. Great care was given during dissection to avoid transection and maintain the structural integrity of each RLN in all specimens. The RLN trunk was identified in the tracheoesophageal groove just inferior to the level of the cricoid cartilage. The trunk of the RLN was followed superiorly using blunt dissection until the first three branches of the RLN were clearly visible. For each dissected nerve

specimen, the branching pattern was photographed and drawn for subsequent categorical analysis.

Dissection and MicroScribe Digitization

Thirty-two RLNs were dissected from the level of the posterior inferior border of the thyroid cartilage distally until the primary nerve branches were easily observable. During each dissection, the utmost care was used to prevent displacement of RLNs from surrounding fascia and tissue. This insured that the precise location of each nerve was preserved for the microScribe digitization process. With each specimen, the RLN trunk was identified proximal to the point at which it enters the tracheoesophageal groove, and tunneled distally exposing the most superficial surface of each nerve branch while leaving the lateral and deep aspects of the nerve imbedded in fascia. A MicroScribe G apparatus was used to digitize the 3 dimensional location within the larynx of each of our 32 RLN specimens. Each RLN trunk was digitized in 1mm increments starting at the level of the posterior inferior border of the thyroid cartilage distally through primary and in many cases secondary branching. The medial and inferior borders of the ipsilateral thyroid cartilage, the epiglottis, and the line of cricoid cartilage visible at the midline of the PCA were also digitized along with each nerve specimen to insure accurate spatial placement of RLNs during the generation of our 3D models.

Heat Mapping

The data points acquired from RLN digitization were imported into Maya software, Autodesk, and used to create 3D renderings of each of our 32 nerve specimens. To create figure 2.2 data from each nerve was fit onto a rendering of a porcine larynx to show the 3 dimensional location of the RLN as it relates to other laryngeal structures. The digitized lines corresponding to the thyroid cartilage and epiglottis were used as reference structures as each nerve was fitted onto the larynx scaffold to insure the accuracy of structure sizes, and spatial location ratios.

Adobe Photoshop CC was used to overlay images of the superior aspect of each of the 32 3D RLN models generated in Maya. As each image was added to the composite image it was warped until the reference structures (thyroid cartilage and epiglottis) were lined up to insure accurate image placement. The composite image color was then altered to generate a heat map which qualitatively shows the likelihood of finding an RLN branch in a given location as seen in figure 2.3.

Results

Porcine Recurrent Laryngeal Nerve Anatomical Variations

Twenty eight nerve dissections revealed three common RLN branching patterns in the pig. Primary branching varied in location of bifurcation from the RLN trunk and in the total number of branches. The lateral secondary RLN branch innervated the interarytenoid, thyroarytenoid, and lateral cricoarytenoid muscles in various terminal distributions to facilitate vocal fold adduction. Innervation of the posterior cricoarytenoid muscle was conserved among all specimens via projections of the medial primary branch of the RLN trunk but we observed substantial distal variation in branching before branch termination into the muscles of the larynx. Figure 2.1 exhibits the three main variations of primary RLN branching in the pig.

Our data suggests that of the three primary porcine branching patterns, A is the most common, being found in 44% of larynges dissected. Specimens exhibiting branching pattern A all possessed the following attributes; the most proximal branch to diverge from the RLN trunk was a medial primary branch which bifurcated into two secondary branches both of which clearly went on to innervate the PCA muscle. The second branch to arise from the RLN trunk was a lateral primary branch that split into various small terminal branches all of which ran away

from the PCA to innervate the laryngeal adductor muscles. Distal to the lateral primary branch the middle primary branch and also innervated the intrinsic laryngeal adductor muscles.

The second most common pattern, B, in which three primary branches (medial, middle, and lateral) arose from the RLN trunk simultaneously, occurred in 32% of our specimens. In all specimens of pattern B, the medial primary branch innervated the PCA along with half of the terminal branches of the middle primary branch. The other half of the terminal branches of the middle primary branch ran away from the PCA and targeted adductors along with the lateral primary branch.

Pattern C, was found in 24% of our specimens. RLNs that exhibited branching pattern C possessed two primary branches, one medial and one lateral arising from the RLN trunk concurrently. The medial of these two branches further diverge into a superior, middle, and inferior secondary branches as it projects toward the PCA. The most superior of these secondary branches appeared to run supero-laterally and possibly innervated vocal fold adductors, whereas the middle and inferior secondary branches clearly innervated the PCA.

3D Laryngeal Mapping

Thirty-two RLN specimens and their reference structures were carefully digitized with a MicroScribe G robotic arm. The microScribe data for each nerve and reference structures, were imported into Maya, Autodesk, and converted into 3D models. After each of the 32 nerves was carefully fit onto an individual larynx scaffold rendering three bilateral larynges were selected for inclusion in figure 2.2. Each of the three larynges selected represent one of the three major RLN primary branching patterns found in the pig. Each row of Figure 2.2 contains three images for each of the three major branching patterns. In the first column there is one cadaveric image with the trunk and branches of the RLN highlighted, followed by best view images (left and right) of our 3D larynx rendering. Please note that the cadaveric image and the rendering images

are not of the same specimen but are representative of the same primary RLN nerve branching pattern. Each row of figure 2.2 accurately shows where the recurrent laryngeal nerve sits within the larynx. 3D larynx renderings and each of our 31 different RLNs can be freely viewed through The National Repository for Laryngeal Data which can be freely accessed at www.nrld.org.

Heat Maps

Figure 2.3 A and 2.3B, describe the relative spatial location of each RLN within the larynx and represents the probability of finding the RLN in a given area. The left and right columns of figure 2.3 represent the right and left RLN specimens respectively. Our data shows that the RLNs on the right side of the larynx have a more consistent and predictable medial/ lateral location as indicated by the solid red areas in figure 2.3B. The RLNs on the left side of the larynx display higher variability in RLN trunk and branch location. In panels C and D each individual distal RLN trunk rendering was overlaid and aligned with one another to show the spatial location viability of the RLN primary branches when registered together.

Discussion

Figure 2.3 is a heat map showing the relative spatial relationships of 32 RLNs when registered together. When considering the entire RLN as a whole our data suggests that the medial/lateral position of the nerve is more consistent on the right than the left side of the larynx as shown in panels A and B. This information is important in several ways. Firstly, the variability of left RLN location could make it more vulnerable to accidental transection during head and neck surgery. If the human larynx were to possess a similar dichotomy between the right and left RLN it needs to be included in surgical planning to avoid accidental damage. This finding is also relevant when considering phrenic/RLN anastomosis for PCA reinnervation surgery. Because the variability of nerve position is greater on the left it could be more difficult

to use left RLNs in PCA reinnervation via phrenic nerve anastomosis. It has been shown that the left phrenic nerve is the best choice to use in an RLN anastomosis procedure[1].

Our data suggests the right RLN is an easier choice for anastomosis in porcine experimental surgeries because its position is more consistent. Unfortunately the right RLN, which is more consistently located is contralateral to the left phrenic nerve. Panels C and D show the spatial variations that exist in just the primary branching pattern of the porcine RLN. It is interesting to note that although the right RLN as a whole is more consistently found in the same place, the primary branches of right RLNs exhibit much more variation in location. The branches on the left RLNs are quite congruent. Not only are they consistent in branch location but left specimens are often found to display the same anatomical branching pattern. Larynx renderings presented in figure 2.2 were created to be useful to those groups studying PCA reinnervation techniques in a pig model. If models like those in this study were created using human larynges they could be used in surgical planning and may decrease the number of accidental RLN transections during surgery.

Acknowledgements
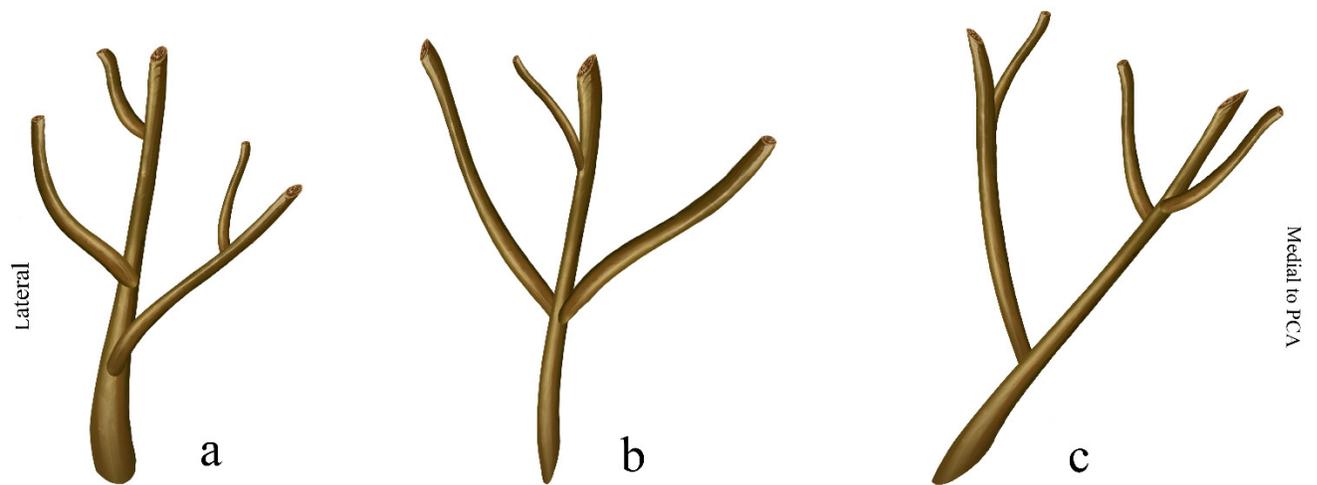
Figure 2.1: The Three Prevailing Branching Patters of the Porcine Recurrent Laryngeal Nerve. 25 specimens were dissected and analyzed. A. The most common variation of the RLN was found in 44% of larynges documented. B. The second most common RLN branching pattern was found in 32% of larynges. C. The least common RLN branching pattern was found in 24% of larynges.
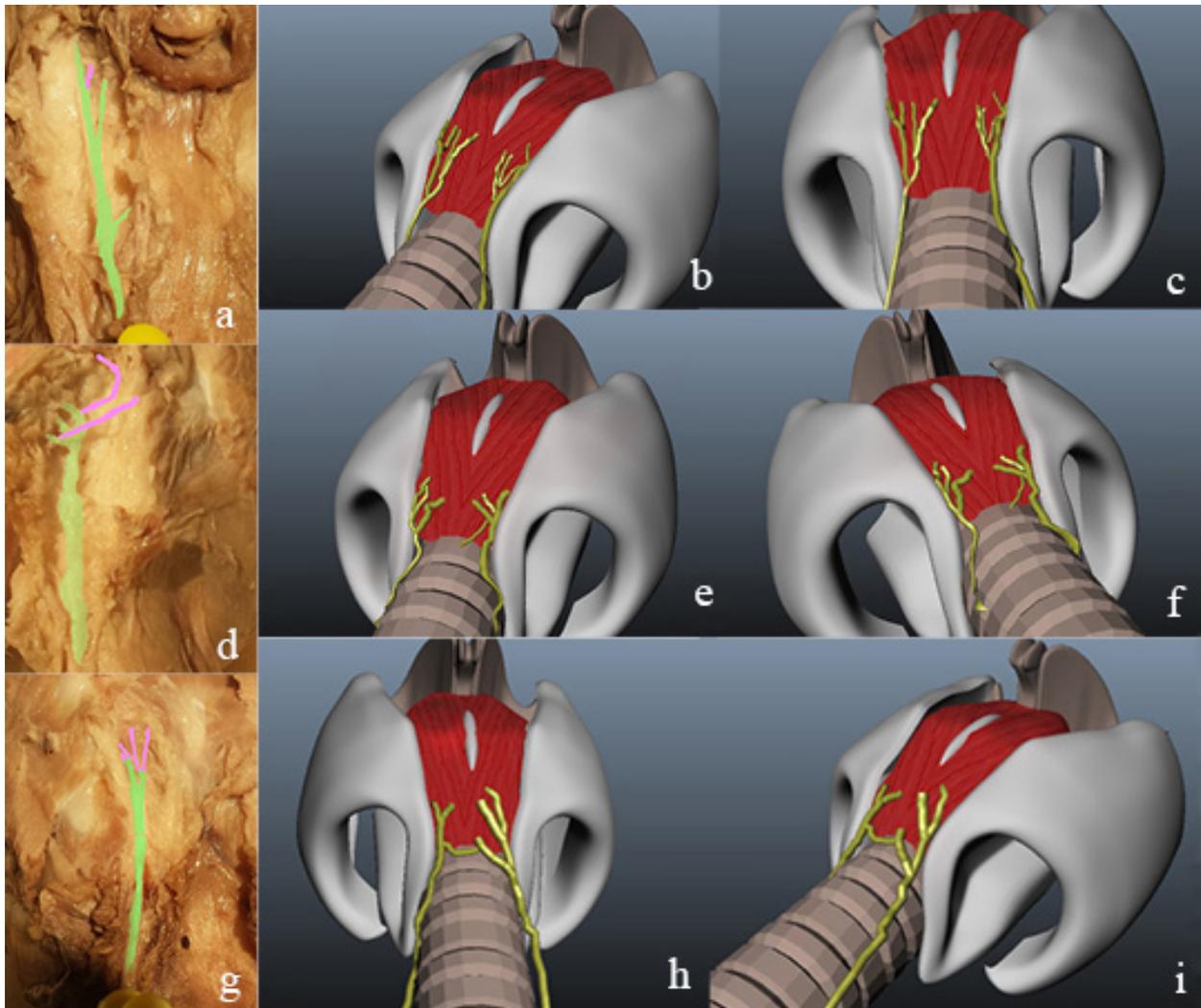
Figure 2.2: Images of Cadaveric Porcine Larynx Specimens that are Representative of the Three Major RLN Branching Patterns. Cadaveric images are accompanied by 3D renderings showing precise RLN placement in relation to other structures within the larynx .Images of branching pattern A, the most common porcine branching pattern (a-c). The nerve has been highlighted for clear viewing, with the RLN trunk and primary branching shown in green and secondary branches shown in purple. Images of branching pattern B, the second most common pattern (d-f). Images of branching pattern C, the least common pattern (g-i)
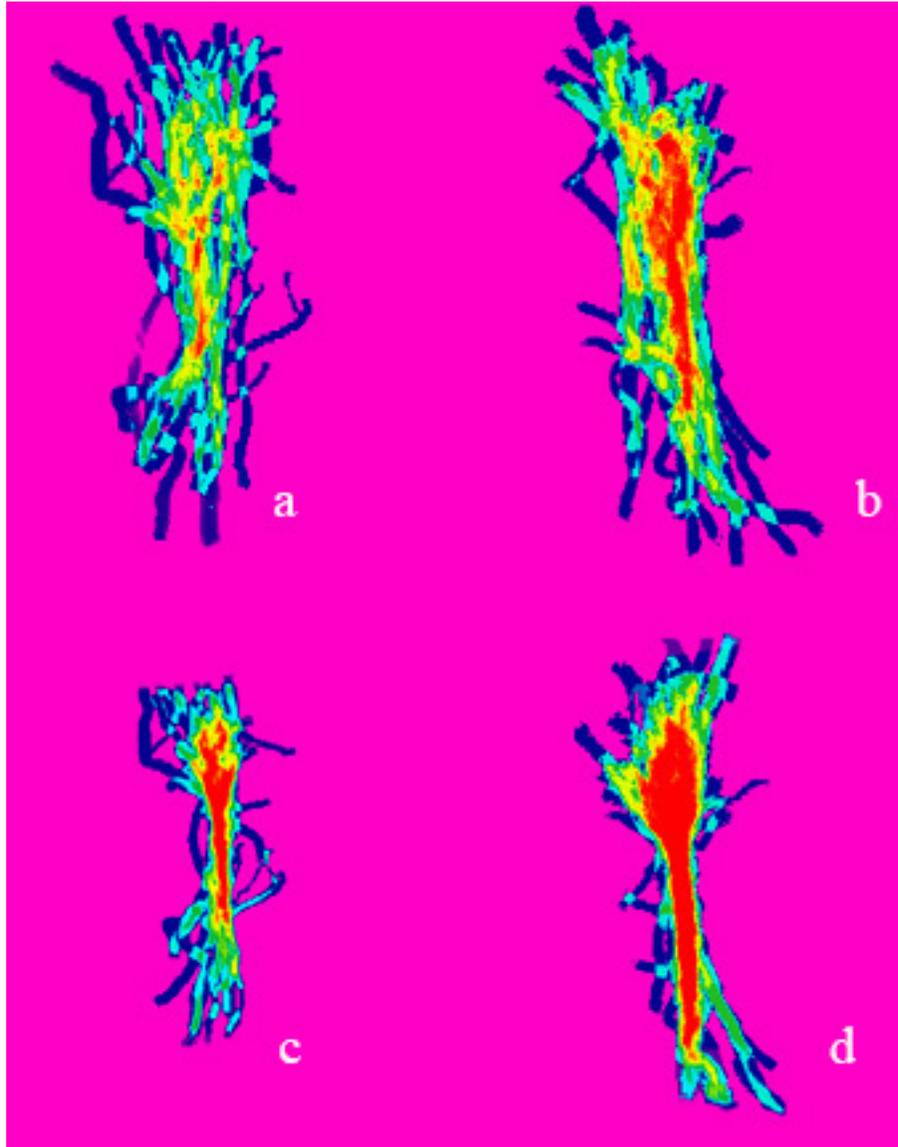
Figure 2.3: A Heat Map Depicting the Relative Spatial Variability from one RLN Specimen to the Next, n=28. The left column contains left nerve specimens and the right column contains right nerve specimens. The relative spatial location of all the left (a) and right (b) RLN's. A comparison of RLN primary branching patterns amongst left (c) and right (d) RLN's after the trunks were registered together.

References

1. Coll DM, Herts BR, Davros WJ, Uzzo RG, Novick AC. 2000. Preoperative Use of 3D Volume Rendering to Demonstrate Renal Tumors and Renal Anatomy 1. Radiographics 20(2):431-438.

2. Crumley R. 1983. Phrenic nerve graft for bilateral vocal cord paralysis. The Laryngoscope 93(4):425-428.

3. Gorti GK, Birchall MA, Haverson K, Macchiarini P, Bailey M. 1999. A preclinical model for laryngeal transplantation: anatomy and mucosal immunology of the porcine larynx. Transplantation 68(11):1638-1642.

4. Jacobs I, Sanders I, Wu B, Biller H. 1990. Reinnervation of the canine posterior cricoarytenoid muscle with sympathetic preganglionic neurons. The Annals of otology, rhinology, and laryngology 99(3 Pt 1):167-174.

5. Jiang JJ, Raviv JR, Hanson DG. 2001. Comparison of the phonation-related structures among pig, dog, white-tailed deer, and human larynges. ANNALS OF OTOLOGY RHINOLOGY AND LARYNGOLOGY 110(12):1120-1125.

6. Knight MJ, McDonald SE, Birchall MA. 2005. Intrinsic muscles and distribution of the recurrent laryngeal nerve in the pig larynx. European archives of oto-rhino-laryngology : official journal of the European Federation of Oto-Rhino-Laryngological Societies 262(4):281-285.

7. Lawler LP, Fishman EK. 2001. Multi–Detector Row CT of Thoracic Disease with Emphasis on 3D Volume Rendering and CT Angiography 1. Radiographics 21(5):1257-1273.

8. Li M, Chen S, Zheng H, Chen D, Zhu M, Wang W, Liu F, Zhang C. 2013. Reinnervation of bilateral posterior cricoarytenoid muscles using the left phrenic nerve in patients with bilateral vocal fold paralysis. PloS one 8(10):e77233.

9. Sanders I, Wu B-L, Mu L, Li Y, Biller HF. 1993. The innervation of the human larynx. Archives of Otolaryngology–Head & Neck Surgery 119(9):934-939.

10. Stavroulaki P, Birchall M. 2001. Comparative study of the laryngeal innervation in humans and animals employed in laryngeal transplantation research. The Journal of Laryngology & Otology 115(04):257-266.

11. van Lith-Bijl JT, Stolk RJ, Tonnaer JA, Groenhout C, Konings PN, Mahieu HF. 1998. Laryngeal abductor reinnervation with a phrenic nerve transfer after a 9-month delay. Archives of Otolaryngology–Head & Neck Surgery 124(4):393-398.

CHAPTER 3: Use of High-Resolution Magnetic Resonance Imaging to Reconstruct Recurrent Laryngeal Neurovascular Structures in 3D

Authors:
Nena Lundgreen Mason[1], Scott Robison[1], Haonan Wang[2], Jonathan J. Wisco Ph.D.[1, 3]

Affiliations
[1]Department of Physiology and Developmental Biology, Neuroscience Center, Brigham Young University, Provo UT
[2]Department of Electrical and Computer Engineering, Brigham Young University, Provo UT
[3]Department of Neurobiology and Anatomy, University of Utah School of Medicine, Salt Lake City, UT

Corresponding Author:

Nena Lundgreen Mason

Department of Physiology and Developmental Biology
Brigham Young University
Laboratory for Translational Anatomy of Degenerative Diseases and Developmental Disorders
4005 LSB Provo, UT 84602-1231

Phone: 208-249-0558
Fax: 801-422-0700
Email: nenalundgreen@gmail.com

Abstract

Recurrent laryngeal nerve (RLN) palsy is a common post-operative complication of many head and neck surgeries. RLN damage often occurs because its location in the tracheoesophageal groove places it at risk for compression or transection during an anterior surgical approach to the cervical spine. Additionally, RLN branching pattern and structure varies substantially from patient to patient, with no established location probability. There is great need for a diagnostic imaging method that can be used to view the specific anatomy of a particular patient for surgical planning in order to minimize complications. Current literature has shown that the pig is an excellent model for human laryngeal anatomy and physiology. [20, 21]

In this study, porcine cadaveric larynx specimens were used to develop several high-resolution MR imaging sequences that yield clear images of the RLN and its accompanying vasculature, as it courses along the tracheoesophageal groove, and branches to innervate the intrinsic muscles of the larynx. The purpose of acquiring these images was to use them to model the three-dimensional (3D) structure of each individual specimen's neurovascular tree using segmentation techniques. We present 25 3D models of porcine laryngeal neurovascular structure. Models were generated via segmentation of images using Amira (FEI, Inc). We intend to optimize our imaging protocols for use on human patients as a diagnostic imaging technique to augment surgical planning.

Introduction

Recurrent laryngeal nerve (RLN) palsy is a common post-operative complication of many head and neck surgeries that has been observed for many years.[10, 19, 20] A study published in 1985 reviewed the cases of 1026 patients that had undergone thyroid gland surgery. Out of those patients, 5.9% suffered from either transient or permanent RLN palsy.[20] A more recent study published in 2000 reported on a set of patients that had undergone either full or

partial thyroidectomy. Of the patients in this study there were 787 RLN's that were in danger of compression or dissection. Thirty-three of these patients or 6.6% incurred RLN damage postoperatively.[21]

RLN damage often occurs because its location places it in a high risk area for compression during an anterior surgical approach to the cervical spine.[22] The RLN is also close in proximity to the thyroid gland, and is often transected or compressed during dissection of the gland.[23] Additionally, RLN branching pattern and structure varies substantially from patient to patient.[7, 11] There are investigators attempting to view the RLN with ultrasound for diagnostic purposes[24, 25] but we suggest that MRI will provide much higher quality imaging and a more definitive 3D representation of RLN location within the larynx. High resolution MRI has been successfully used to clearly view and characterize pathologies of small peripheral nerves in many studies as 3T magnets have become more readily available to researchers and clinicians.[26-28]

Magnetic resonance neurography is a well-established technique that has been used for many years and many purposes.[29-33] There is great need for a diagnostic imaging method that can be used to view the specific laryngeal anatomy of a particular patient prior to surgery to minimize complications. In this report, we will show that high resolution MRI can be used in such a capacity to identify the exact location of the RLN with its accompanying vasculature and generate 3D models to augment surgical planning. Current literature has shown that the pig is an excellent model for human laryngeal anatomy and physiology.[13-15] In this study, porcine cadaveric larynx specimens were used to develop high-resolution MR imaging sequences that yield clear images of the RLN and it's accompanying vascular tree as it courses along the tracheoesophageal groove and branches to innervate the intrinsic muscles of the larynx.

The purpose of obtaining these images is to use them to model the three-dimensional (3D) structure of each individual neurovascular tree via MR image segmentation. We present 25 3D models of porcine structure derived from the segmentation of high-resolution MR images. Models were generated via segmentation of images using Amira (FEI, Inc.). We establish that high resolution MRI is a potential tool that can enable clinicians to augment surgical planning by determining the structure of a specific patient's RLN in a non-invasive manner.

Materials and Methods

Imaging protocol 1 (Segmentation, High Resolution):

Twenty-five cadaveric excised porcine larynx specimens were suspended in 3% agar and high resolution images were acquired with a 3 Tesla (T) Siemens MRI scanner, and a standard 32 channel head coil. The repetition time (TR), echo time (TE), and field of view (FOV) used to acquire our images was chosen to yield high signal to noise ratio (SNR) efficiency while maintaining maximal contrast between tissues of interest in the larynx, particularly the bilateral recurrent laryngeal nerves and accompanying vasculature. Scan parameters were as follows: Averages= 4, TR= 14, TE=4.96, FOV= 128, Voxel Size= 0.3x0.3x0.5mm. Acquisition time for scan protocol 1 was 28 minutes and 2 seconds.

Imaging protocol 2 (Imaging Titration, Lower Resolution):

In order achieve image resolution quality similar to imaging protocol 1 but maintain clinically relevant scan parameters, our second lower-resolution scan protocol employed a three-dimensional (3D) FLASH sequence. Imaging protocol 2 was developed on the same 3T Siemens whole-body scanner. The resolution of imaging protocol 2 was lowered by altering the following parameters used in imaging protocol 1. The FOV was set at 128 mm (readout) x 84 mm (phase) x

96 mm and the acquisition matrix was 256 (readout) x 168 (phase encode) and 240 in slices direction (38 slices were acquired for oversample to reduce image aliasing) which yielded the voxel size equal to 0.5 x 0.5 x 0.5mm. The TR/TE = 14/4.96 msec, total scan time was 7 minutes and 32 seconds, and the flip angle was 25 degrees. Other acquisition parameters were readout bandwidth = 180 Hz/pixel, a fast mode slab selective RF pulse was also employed to further reduce aliasing.

Segmentation:

MR images of each larynx specimen were manually segmented based on signal intensity using Amira (FEL, Inc.). The RLN distinguished from surrounding laryngeal tissue via differences in image contrast, and was carefully highlighted in each image slice. Vascular trees in close proximity to the RLN were also identified and segmented. Highlighted nerve and vascular tissue from each slice were used to render a 3D model of each specimen's unique RLN structure along with its accompanying vascular tree. Please note that both neuro and vascular structures found within postmortem laryngeal tissue have similar signal intensity.

Results

We have engineered several scanning protocols using a 3T Siemens MRI scanner that produce clear images of the RLN and its accompanying vasculature. Both neural and vascular tissue are easily distinguishable in images produced with all our scan protocols (see Figure 3.1), but have the same signal intensity, and thus difficult to distinguish from one another. Figure 3.2 displays the segmented neurovascular tree *in situ* within the segmented porcine larynx (rendered translucent for visualization). It is clear the entire vascular tree, RLN trunk, and branches have been captured by our MR imaging sequences. Figure 3.3 shows 3D mapping of the bilateral RLN and its accompanying vascular tree in six specimens that highlight the many anatomical

variations that occur in porcine RLN and vascular branching. Images in Figure 3.3 were generated via careful segmentation of our MR images acquired with imaging protocol 1. Twenty-five total specimens were segmented successfully and 3D maps of all neurovascular structures were generated. The six particular specimens shown in Figure 3.3 were selected because they represented the many different pattern variations of porcine neurovascular trees in our sample.

Figure 3.4 contains two images acquired following a resolution titration of imaging protocol 1. The image in panel B was acquired with our lower resolution imaging protocol 2 following titration. Imaging protocol 2 was designed to maximize nerve and vascular contrast from surrounding laryngeal structures, while maintaining scan parameters that yield a clinically relevant scan protocol. Both panel A and panel B contain axial slices acquired from the same excised porcine larynx specimen at the same vertical level. The image in panel A was acquired with our higher resolution imaging protocol 1 (see Methods section). In both panels 3 clusters of high intensity voxels are visible. These clusters are indicative of neurovascular structures on the right side of the larynx as indicated by white arrows. The partial voluming seen in panel B due to the larger voxel size which yields diminished intensity but decreased scan time.

Discussion

Our MRI sequences produce images of the laryngeal neurovascular tree with sufficient clarity to easily view all neuronal and vascular branching. Although in each of our images neuronal and vascular structures have the exact same contrast we suggest that a gadolinium contrast agent may be used clinically prior to diagnostic scans to make nerve/vessel differentiation clear. Gadolinium has been successfully used in many MR imaging studies to produce sharp contrast in vascular structures.[34-36] In all of the images we acquired the relationship between the RLN and its accompanying vasculature and surrounding laryngeal

structures could easily be identified bilaterally if a simple contrast agent is employed prior to scanning. With the addition of a contrasting agent our images could be used determine which anatomical branching pattern is present in a given specimen without dissection. This imaging method could serve as a valuable diagnostic technique to determine surgical candidacy and augment surgical planning since our results demonstrate a tight spatial correlation between nervous and vascular structures.

MR Image Segmentation and 3D Modeling of Laryngeal Neurovascular Structures

Figure 3.3 shows six bilateral neurovascular trees that were generated via image segmentation of high resolution MR images of six individual porcine larynx specimens. In each of our 25 total larynx specimens the intricate detail of neurovascular tree structure was fully captured via MR image segmentation. These six particular specimens shown in figure 3.3 were chosen for display because they are representative of the many different pattern variants that porcine neurovascular trees in our sample population comprise. The level of detail we were able to capture in our models (see Figure 3.3) allows us to state with confidence that the entirety of primary and in many cases secondary branching of the RLN is fully represented. This segmentation technique could easily be used to create individualized models of laryngeal neurovascular anatomy for specific patients augment surgical planning if a simple contrast was used prior to scanning.

MRI Contrast and Titration

The results of our imaging titration experiment (see Figure 3.4) show that clinically relevant scan protocols can be used to generate individualized mapping of the RLN and accompanying vasculature because both panels A and B offer clear viewing of neurovascular structures within the porcine larynx. Our main concerns in the development of imaging protocol 2

were shortening the scan time and minimizing the specific absorption rate. In practice, we attempted to restrict the scan time to less than 10 minutes to reduce any motion artifacts that may arise during an in-vivo scan. We decreased the matrix size which sacrificed some image resolution but yielded a shorter scan time. Despite the sacrifices made in resolution imaging protocol 2 still maintained a 0.5mm isotropic resolution. We report that we were still able to track structures of interest within the larynx, including the RLN and surrounding vascular structures in sufficient detail to generate satisfactory segmentations despite the lower resolution of imaging protocol 2.

Future Directions

All of our scan protocols were optimized for use with a 32-channel head coil. We acknowledge that a 32-channel head coil could not be used to acquire images of a patient's larynx because its shape won't allow adequate coverage of the neck. We further acknowledge that generating images like the ones acquired in this report on a live patient would result in complications such as image aliasing from surrounding structures within the neck. However, we suggest that a surface coil could be employed with a similar imaging sequence to our low resolution scan protocol on living person with good results. Additionally a surface coil placed on the anterior aspect of the neck of a living human subject would be able to move with the patient and thus eliminate excessive image noise caused by normal physiologic movements.

Furthermore, when using a surface coil, longer scan acquisition times may be better tolerated since subject movement-generated noise would be decreased which could yield images with better image contrast and resolution. We advise any larynx imaging protocol adapted from our imaging sequences for use with a surface coil be designed to insure that their new SNR mirrors that of our imaging protocols. This could be accomplished by taking the signal intensity over the area of interest as obtained with the surface coil and dividing by the standard deviation

of any background noise. We plan to explore the use of our imaging sequences on living human

subjects further with the use of a surface coil in future studies.

Figure 3.1: A MR Image of a Porcine Larynx Slice Taken in the Frontal Plane. This image displays the clarity with which our MRI scanning protocols can capture the RLN. A large portion of the right recurrent laryngeal nerve (circled in red) is easily seen within this single image slice.
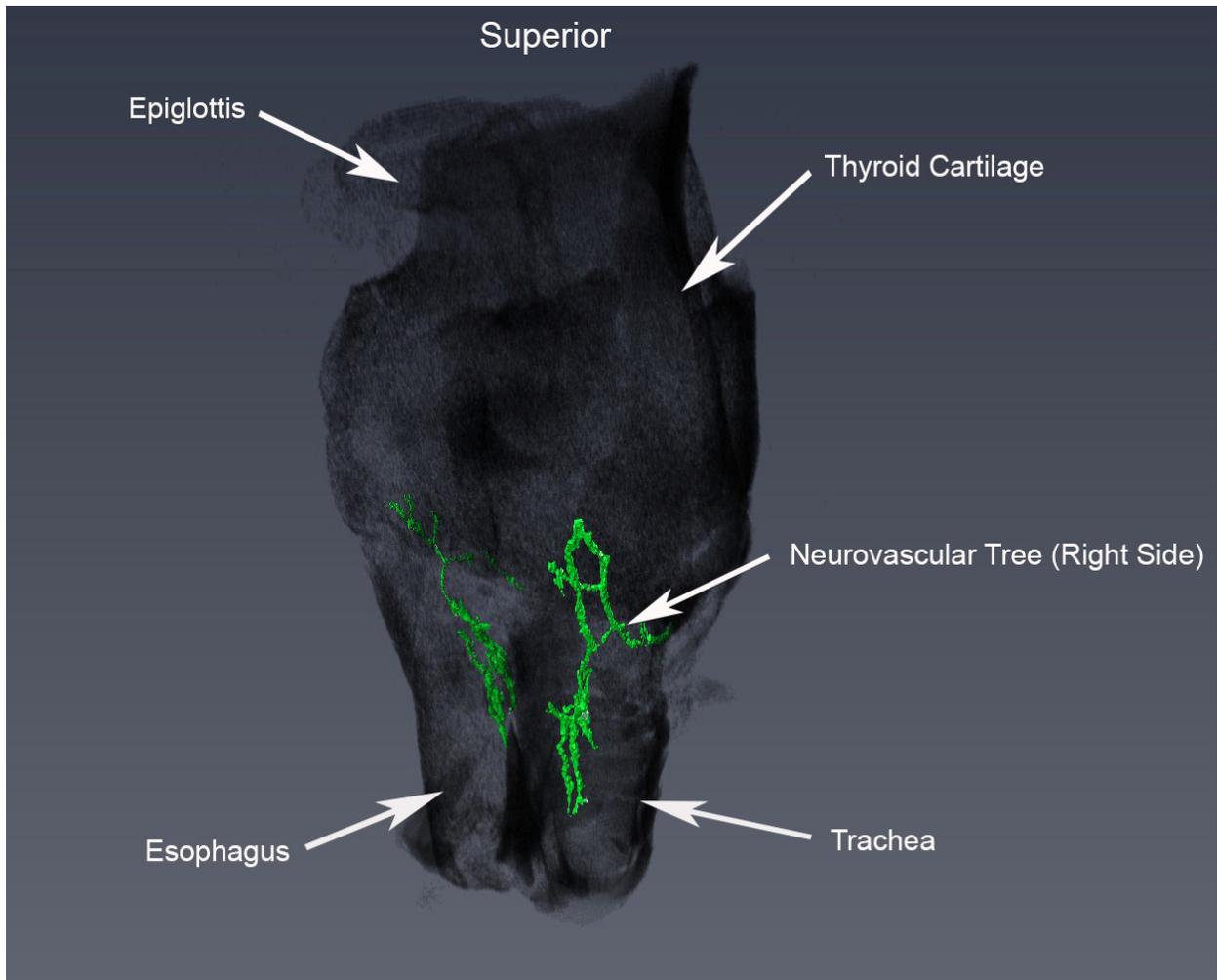
Figure 3.2: The Segmented Recurrent Laryngeal Neuroanatomy and Accompanying Vasculature In Situ within the Tracheoesophageal Groove of the Porcine Larynx Bilaterally.
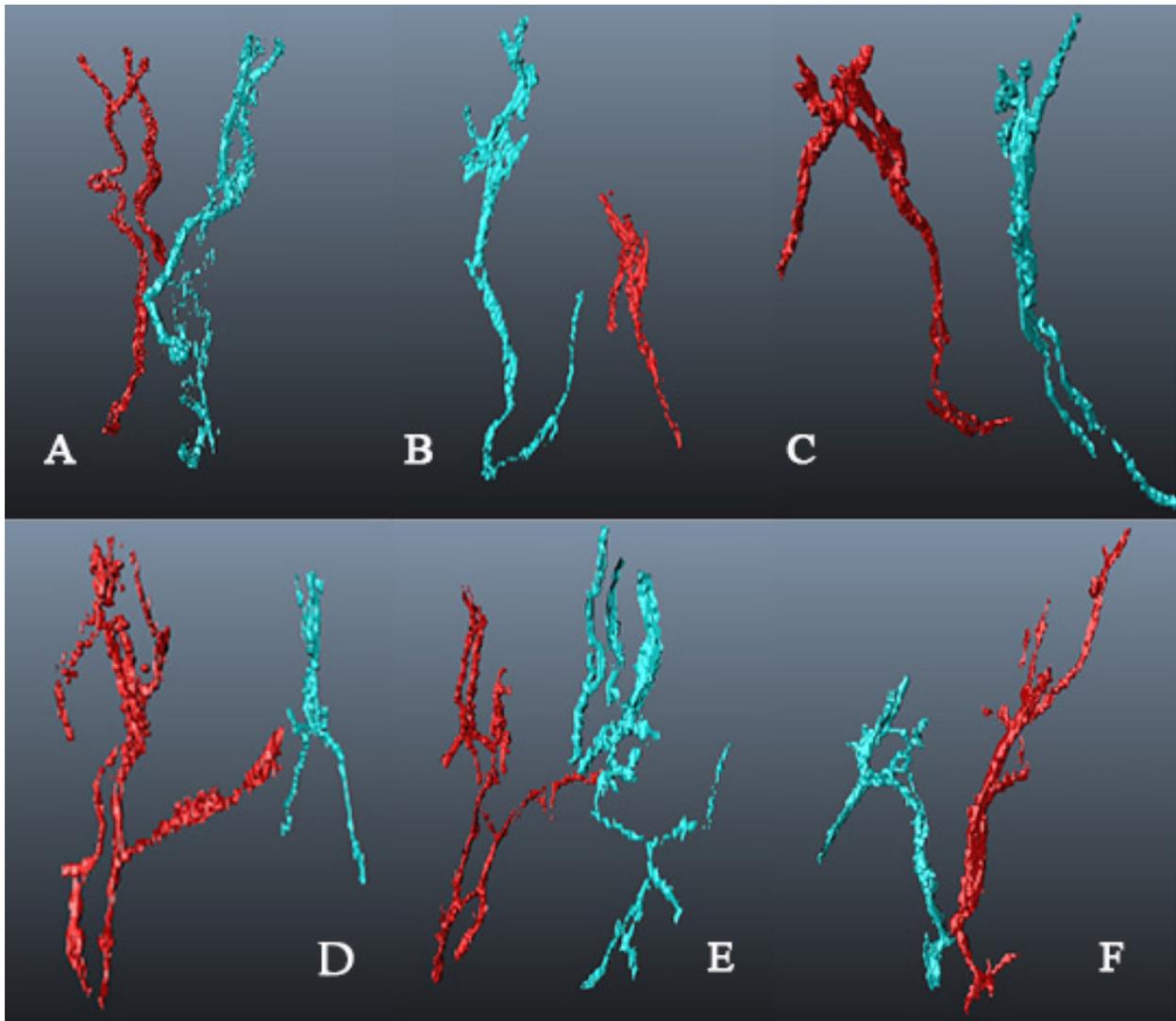
Figure 3.3: Six Models Generated via Segmentation of the RLN and Accompanying Vasculature of 6 Bilateral Specimens that Show True In Situ Placement within the Porcine Larynx. The neurovascular tree located on the right side of each specimen are indicated in red and the left side in blue. These particular six specimens were chosen because they best display the structural variation exhibited in porcine RLN and vasculature structure. Each model was rotated to offer the best view of both the right and left sides. In each panel the RLN trunk (inferior) begins at the bottom of the panel and branches near the top (superior).
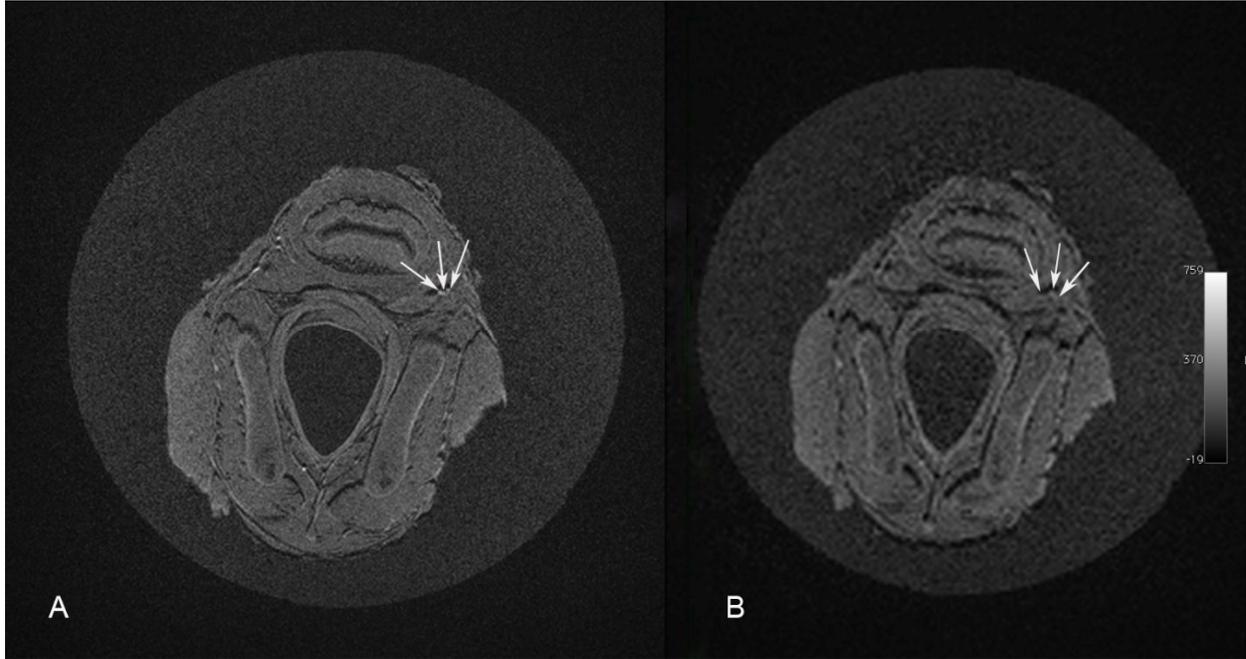
Figure 3.4: The Results of an Imaging Contrast Titration Experiment. The MR image in panel A was acquired using our higher resolution imaging protocol 1. Panel B shows an MR image acquired with our lower resolution imaging protocol 2. Both image slices are axial slices of the same excised porcine larynx specimen and are taken from the exact same level vertically. In both panels A and B the same three neurovascular structures are visible as indicated by three white arrows.

References

1. Chiang F-Y, Wang L-F, Huang Y-F, Lee K-W, Kuo W-R: Recurrent laryngeal nerve palsy after thyroidectomy with routine identification of the recurrent laryngeal nerve. Surgery 2005, 137(3):342-347.

2. Li M, Chen S, Zheng H, Chen D, Zhu M, Wang W, Liu F, Zhang C: Reinnervation of bilateral posterior cricoarytenoid muscles using the left phrenic nerve in patients with bilateral vocal fold paralysis. PloS one 2013, 8(10):e77233.

3. H, Terins J: Recurrent laryngeal nerve palsy in thyroid gland surgery related to operations and nerves at risk. Archives of surgery 1985, 120(4):475-477.

4. Lo C-Y, Kwok K-F, Yuen P-W: A prospective evaluation of recurrent laryngeal nerve paralysis during thyroidectomy. Archives of surgery 2000, 135(2):204-207.

5. Apfelbaum RI, Kriskovich MD, Haller JR: On the incidence, cause, and prevention of recurrent laryngeal nerve palsies during anterior cervical spine surgery. Spine 2000, 25(22):2906-2912.

6. Jatzko GR, Lisborg PH, Müller M, Wette VM: Recurrent nerve palsy after thyroid operations--principal nerve identification and a literature review. Surgery 1994, 115(2):139-144.

7. Ardito G, Revelli L, D'Alatri L, Lerro V, Guidi ML, Ardito F: Revisited anatomy of the recurrent laryngeal nerves. The American journal of surgery 2004, 187(2):249-253.

8. Damrose EJ, Huang RY, Ye M, Berke G, Sercarz JA: Surgical anatomy of the recurrent laryngeal nerve: implications for laryngeal reinnervation. The Annals of otology, rhinology, and laryngology 2003, 112(5):434-438.

9. Deveze A, Sebag F, Hubbard J, Jaunay M, Maweja S, Henry J-F: Identification of patients with a non-recurrent inferior laryngeal nerve by duplex ultrasound of the brachiocephalic artery. Surgical and Radiologic Anatomy 2003, 25(3-4):263-269.

10. Solbiati L, De Pra L, Ierace T, Bellotti E, Derchi L: High-resolution sonography of the recurrent laryngeal nerve: anatomic and pathologic considerations. American journal of roentgenology 1985, 145(5):989-993.

11. Thawait S, Chaudhry V, Thawait G, Wang K, Belzberg A, Carrino J, Chhabra A: High-resolution MR neurography of diffuse peripheral nerve lesions. American Journal of Neuroradiology 2011, 32(8):1365-1372.

12. Bendszus M, Stoll G: Technology insight: visualizing peripheral nerve injury using MRI. Nature clinical practice neurology 2005, 1(1):45-53.

13. Aagaard BD, Lazar DA, Lankerovich L, Andrus K, Hayes CE, Maravilla K, Kliot M: High-resolution magnetic resonance imaging is a noninvasive method of observing injury and recovery in the peripheral nervous system. Neurosurgery 2003, 53(1):199-204.

14. Filler AG, Kliot M, Howe FA, Hayes CE, Saunders DE, Goodkin R, Bell BA, Winn HR, Griffiths JR, Tsuruda JS: Application of magnetic resonance neurography in the evaluation of patients with peripheral nerve pathology. Journal of neurosurgery 1996, 85(2):299-309.

15. Chhabra A, Lee PP, Bizzell C, Soldatos T: 3 Tesla MR neurography—technique, interpretation, and pitfalls. Skeletal radiology 2011, 40(10):1249-1260.

16. Filler A, Kliot M, Winn H, Tsuruda J, Hayes C, Howe F, Griffiths J, Bell B: Magnetic resonance neurography. The Lancet 1993, 341(8846):659-661.

17. Chhabra A, Subhawong TK, Bizzell C, Flammang A, Soldatos T: 3T MR neurography using three-dimensional diffusion-weighted PSIF: technical issues and advantages. Skeletal radiology 2011, 40(10):1355-1360.

18. Zhang Z, Song L, Meng Q, Li Z, Luo B, Yang Y, Pei Z: High-resolution diffusion-weighted MR imaging of the human lumbosacral plexus and its branches based on a steady-state free precession imaging technique at 3T. American Journal of Neuroradiology 2008, 29(6):1092-1094.

19. Gorti GK, Birchall MA, Haverson K, Macchiarini P, Bailey M: A preclinical model for laryngeal transplantation: anatomy and mucosal immunology of the porcine larynx. Transplantation 1999, 68(11):1638-1642.

20. Jiang JJ, Raviv JR, Hanson DG: Comparison of the phonation-related structures among pig, dog, white-tailed deer, and human larynges. ANNALS OF OTOLOGY RHINOLOGY AND LARYNGOLOGY 2001, 110(12):1120-1125.

21. P, Birchall M: Comparative study of the laryngeal innervation in humans and animals employed in laryngeal transplantation research. The Journal of Laryngology & Otology 2001, 115(04):257-266.

22. H-J, Brasch RC, Press W-R, Wesbey GE: Characteristics of gadolinium-DTPA complex: a potential NMR contrast agent. American Journal of Roentgenology 1984, 142(3):619-624.

23. Carr D, Brown J, Bydder G, Steiner R, Weinmann H, Speck U, Hall A, Young I: Gadolinium-DTPA as a contrast agent in MRI: initial clinical experience in 20 patients. American Journal of Roentgenology 1984, 143(2):215-224.

24. Revel D, Loubeyre P, Delignette A, Douek P, Amiel M: Contrast-enhanced magnetic resonance tomoangiography: a new imaging technique for studying thoracic great vessels. Magnetic resonance imaging 1993, 11(8):1101-1105

CHAPTER 4: Modeling of the 3D Geometric Structure and Tissue Composition of Human Laryngeal Anatomy via High-Resolution MRI Segmentation and Histological Analysis

Authors:
Nena Lundgreen Mason[1], Haonan Wang[2], Brett Heldt[1], BreAnna Long[1], ReyLynn Reid[1], Amin Nazaran[2], Brett Gardiner[1], Luke Sanders[3], Geoffrey Dorius[3], David Morton Ph.D.[3], Neal K. Bangerter Ph.D.[2], Jonathan J. Wisco Ph.D.[1, 3]

Affiliations:
[1]Department of Physiology and Developmental Biology, Neuroscience Center, Brigham Young University, Provo UT
[2]Department of Electrical and Computer Engineering, Brigham Young University, Provo UT
[3]Department of Neurobiology and Anatomy, University of Utah School of Medicine, Salt Lake City, UT

Corresponding Author:

Nena Lundgreen Mason

Department of Physiology and Developmental Biology at Brigham Young University
Laboratory for Translational Anatomy of Degenerative Diseases and Developmental Disorders
4005 LSB Provo, UT 84602-1231

Phone: 208-249-0558
Fax: 801-422-0700
Email: nenalundgreen@gmail.com

Abstract

Many patients that seek treatment from otolaryngologists or speech pathologists are afflicted with complications pertaining to the anatomy of the phonatory neuromuscular system. In many clinical research scenarios it is appropriate to use a model to understand the anatomy and physiology of the body when the particular area of interest is difficult or dangerous to access in vivo. The anatomical location of the human vocal apparatus renders it particularly difficult to access for the measurement pathological changes, damage assessment, and surgical intervention in patients suffering from phonation related pathologies. Because of it's difficult to access location, laryngeal modeling is a valuable tool for the advancement of modern phonosurgery.

To better understand both the 3D geometric structure of human laryngeal anatomy and the structural attributes of its many tissue components we have acquired high-resolution magnetic resonance (MRI) spatially calibrated images of 9 adult excised human larynx specimens. Additionally we have conducted histological analysis of those same 9 larynx specimens via H&E and Mallory's Trichrome staining techniques to distinguish between, muscle, cartilage, collagen, elastin, and connective tissue. When analyzed together the MR images and the histological slides allow correlation between MR image contrast variation and specific tissue composition. Detailed information regarding vocal fold tissue composition and histological geometry provided by this study will enable laryngeal modelers to select more appropriate and life-like materials with which to construct synthetic vocal fold models. This study may also lay early groundwork in the field of voice research, specifically, the engineering of voice prostheses to be used in laryngoplasty procedures.

Introduction

The discipline of phonosurgery has two primary goals; to improve voice quality and restore lost vocal function. [1] Many patients that seek treatment from otolaryngologists or speech pathologists are afflicted with complications pertaining to the anatomy of the phonatory neuromuscular system.[2] In many clinical research scenarios it is appropriate to use a model to understand the anatomy and physiology of the body when the particular area of interest is difficult or dangerous to access in vivo. Where truly accurate life-like anatomical models are available it is appropriate to use them to determine the outcome of experimental surgical procedures without risking patient safety. The anatomical location of the human vocal apparatus renders it particularly difficult to access for the measurement pathological changes, damage assessment, and surgical intervention in patients suffering from phonation related pathologies. Because of it's difficult to access location, laryngeal molding would serve as a very valuable tool for the advancement of modern phonosurgery.

There have been many attempts to build both functional computational and physical models of the human vocal apparatus [2-10] but so far realistic human phonatory characteristics have not been replicated through modeling. One weakness of models generated thus far is the vast difference between the physical materials selected for model construction and the physical characteristics and complex relationships of the many tissues of the human larynx. The morphology of the various cartilaginous and elastic tissues of the larynx determines each individual's intrinsic muscular action of the laryngeal muscles and in turn their vocal fold geometry. An individual's vocal fold geometry determines their vocal register and unique phonatory characteristics.[7]

Antecedent studies have made progress in identifying specific laryngeal tissue material properties. Particularly, emphasis has been placed on characterizing the stiffness of the vocal folds themselves as measured by either the Shear modulus or the Young's modulus. Several studies have focused on the vocal fold as whole [11], while others target specific layers of the fold itself [12]. There have been numerous other studies that characterize additional laryngeal features such as the vocal ligament and muscular structure among others [13-16]. There are still more questions to answer regarding laryngeal tissue composition and properties however, much less is known about the macroscale geometry of the larynx, and little to no information is available that can accurately relate these two important aspects of laryngeal anatomy together.

To better understand both the 3D geometric structure of human laryngeal anatomy and the structural attributes of its many tissue components we have acquired high-resolution magnetic resonance imaging (MRI) spatially calibrated images of 9 adult excised human larynx specimens. Additionally we have conducted histological analysis of those same 9 larynx specimens via H&E and Mallory's Trichrome staining techniques to distinguish between, muscle, cartilage, collagen, elastin, and connective tissue. When analyzed together the MR images and the histological slides allow correlation between MR image contrast variation and specific tissue composition. Detailed information regarding vocal fold tissue composition and histological geometry provided by this study will enable laryngeal modelers to select more appropriate and life-like materials with which to construct synthetic vocal fold models. This study may also lay early groundwork in the field of voice research, specifically, the engineering of voice prostheses to be used in laryngoplasty procedures.

Materials and Methods

Tissue Specimens:

We acquired all of our human larynx specimens from the University of Utah School Of Medicine Body Donor Program. The specimens were fixed using standard cadaver embalming procedures with 10% paraformaldehyde. The typical post-mortem interval is 48 hours to account for serum testing. Specimens were dissected in the neck and excised using axial infrahyoid (C2-3) and infracricoid (C5-6) cuts. In all specimens the hyoid bone, and the omohyoid, thyrohyoid, cricothyroid, and sternohyoid muscles were removed. Additionally, the trachea was cut away between the first cartilaginous ring and the cricoid cartilage. All Specimens were then stored in a 10% formalin solution until decalcification and imaging. Each larynx was decalcified in a 14.4% EDTA solution for two weeks to prepare them for both tissue processing, and sectioning for histological staining.

Imaging:

Following the removal of all exterior excess muscle all 9 larynx specimens were imaged using a two-dimensional T2 weighted turbo-spin echo sequence. The sequence was implemented on a 3T Siemens whole-body scanner (Siemens Medical Systems, Erlangen, Germany) with a 32-channel head coil. The FOV of the scan is 200 mm (readout) x 141.5 mm (phase) x 1 mm (slice-thickness) and the acquisition matrix was 896 (readout) x 634 (phase encode) and 42 in slices direction with interleave acquisition pattern (12 slices was used for oversample) which yields the voxel size equals to 0.22 x 0.22 x 1mm. Because of the small voxel size, 9 averages were employed to obtain an adequate SNR which made the total acquisition time about 55 minutes. The TR/TE = 5000/89 msec flip angle is 150 degree. Other acquisition parameters were; turbo factor =12, and readout bandwidth = 328 Hz/pixel. Fast mode RF pulse was selected and the slice distance was 1mm.

Segmentation and Modeling:

MR images of each larynx specimen were manually segmented based on signal intensity using Amira (FEL, Inc.). Several laryngeal structures were identified via image contrast and were highlighted in each image slice to discover the 3D geometry of each individual structure and its spatial relationship with surrounding laryngeal structures. The thyroid, cricoid, and arytenoid cartilages were segmented in their entirety in each of our 9 larynx specimens along with the esophagus, vocal fold mucosa, vocal ligament, and vestibular space. Following segmentation 3D models were generated to view each laryngeal structure and analyze its three-dimensional geometry.

Histological Processing and Cutting:

Specimens were submerged in an EDTA decalcifying solution to remove any calcification in the cartilage which would hinder further processing. The decalcifying solution protocol was obtained from Leica Biosystems. Our solution consisted of 10% EDTA by volume brought to a pH of 7-7.5 by addition of sodium hydroxide pellets. Specimens were submersed for 10 days with one change of solution after 5 days. Processing revealed that calcium deposits were still present, so they were again submersed in decalcifying solution, this time consisting of 10% EDTA at a pH of 5-6. Each larynx was sectioned midsagittally to allow better solution penetration. The solution was changed every 5-7 days until specimens were deemed soft by tactile inspection. Total time in EDTA solution ranged from 1-20 days. Specimens were placed in 10% formaldehyde when deemed soft. Each half was cut coronally into 8-11 blocks, 4-6 of which typically contained vocal fold tissue. Blocks were then processed overnight using a xylene-free Leica protocol, embedded in paraffin wax, sliced at 10 microns, and mounted on glass slides for histological staining.

Staining and Imaging:

Slides were stained using either a standard Hematoxylin & Eosin (H&E) or Mallory's

trichrome stain. H&E stain timings for the larynx tissue were determined by stain

experimentation using pig larynx tissue. Our porcine stain experiments indicated that 5 minutes

in hematoxylin before counterstaining in eosin for 30 seconds produced the best results. The

Mallory's trichrome stain was performed as described in the IMEB Inc. kit protocol, hydrating

through alcohols and skipping steps 2 and 3, as our sections were not fixed in mercuric chloride.

High resolution images of the slides at 20X magnification were obtained using a Leica SCN400

scanner at Leavitt Medical.

Results

Models:

Nine 3D models of human laryngeal structure were generated via high resolution MR

image segmentation. Models of laryngeal structure for two specimens can be seen in figures 4.2-

4.5. Models not published in this study can be viewed through The National Repository for

Laryngeal Data which can be freely accessed at www.nrld.org. The 3D structure and relative

spatial location of the vocal fold mucosa, thyroid cartilage, cricoid cartilage, arytenoid cartilage,

vestibular space, vocal ligament, intrinsic laryngeal muscle, and fascial spaces can be clearly

observed as well as their positions relative to one another.

Histological Slides:

Each larynx was bisected midsagittally into right and left halves. Each half was then

sectioned into 1cm axial slices of tissue and then sectioned into 10 micron slices, mounted on

glass histological slides, and stained using either H&E or Mallory's Trichrome staining

protocols. Our histological slides show the cellular components of different laryngeal structures

at various levels from superior to inferior as they lie in the axial plane. Many types of tissue were found to exist within laryngeal structure which can be seen in figure 4.8 such as; mucosal epithelial tissue, skeletal muscle and perimysium, mucus glandular cells, hyaline cartilage, and some areas of bone produced via endochondral ossification remolding as the specimen aged.

Each labeled field from the segmented MR images of our larynx specimens proved to contain several cell types. The area identified as the vocal fold mucosa by homogenous MRI contrast contained a mixture of epithelial, muscular, collagen, elastin, and glandular tissue. Specifically ciliated columnar stratified epithelium, sub-mucosal respiratory glands, skeletal muscle, perimysium fascial spaces, and chronic inflammatory cells within the lamina propria were all seen upon histological analysis of the vocal fold mucosa. Three cartilaginous structures are found within the human larynx the thyroid, cricoid, and arytenoid cartilages. All three cartilages are composed of hyaline cartilage and dystrophic bone. Muscular tissue was shown to contain skeletal muscle and fascial spaces that are mostly perimyseial

Discussion

3D Modeling:

Initially our goal was to capture the whole vocal fold in a single axial slide for histological analysis alongside our axial MR images. The axial plane was selected for MRI of the larynx because the field of view could be restrained to smaller dimensions which allowed for maximal image resolution without losing important structural information. Since our MR images display the larynx in an axial plane only we decided to block and section the tissue for histological analysis in the coronal plane so that the MR images and the histology together would allow a more a 3-dementional analysis of the vocal folds.

When examining our larynx models from inferior to superior a certain level of discontinuity in shape is observed. The reason for this is that each MR image slice that was acquired through our imaging protocol (see methods section) is one millimeter in height and 0.22 millimeters in width and depth. The MRI slices are asymmetrical in voxel dimension which causes the pixels in the models to be 5 times thicker in the X-Y plane as compared to the Z plane. A certain amount of discontinuity is to be expected in the coronal and sagittal planes of our models due to the fact that when our images were acquired they were designed to sacrifice resolution in the coronal plane to maximize resolution and detail in the axial plane.

In regards to the structures labeled "fascia" we would like to mention that these are areas identified via a specific shade of MR image contrast and segmented. Despite the randomness in appearance of their location each modeled fascial space represents spaces between the bellies of individual intrinsic laryngeal muscles and in some cases perimyseial layers between muscular fascicles. Labeled fascial spaces represent the spatial location of intermuscular fascial pockets that are sufficiently thick to be identified by MR image contrast alone. These results were substantiated by histological analysis of our larynx specimens following imaging.

Integration of Laryngeal Histological Analysis and 3D Modeling:

Current MRI technology is not advanced enough to distinguish between distinct tissue and cell types that are found close together and in small quantities. However, high resolution MRI can be used to successfully identify what groups of general tissue types exist in a structure with only image contrast. In this study correlations between our 3D models and histological slides allow us to make connections between MR image contrast and tissue types.

Each colored structure seen on our 3D models was painstakingly segmented in each MR image slice based on differences in image contrast. Histological slides of the same larynx

specimens were analyzed to determine what tissue and cell types are found in different laryngeal structures. Figure 4.1 correlates laryngeal structures identified via image contrast and structures seen on histological analysis. It is our intent that our 3D models and histological slides of the human larynx be used to correlate 3D structural shape with specific tissue type. This can be accomplished by examining the models in panels A-E in figure 4.3, Identifying a specific structure using the color key in figure 4.3 panel F, and finally determine the tissue and cellular components of that specific laryngeal structure as displayed in Figure4.1.

For example the green structure shown in figure 4.2 panels A-E is identified in panel F as the thyroid cartilage. Table 1 states that the thyroid cartilage is comprised of hyaline cartilage and dystrophic bone. In this manner extrapolations can be made to understand the 3D histological geometry of human laryngeal structure. It is our intention that the detailed information regarding vocal fold tissue composition and laryngeal histological geometry provided by this study will enable laryngeal modelers to select more appropriate and life-like materials with which to construct synthetic vocal fold models. This study may also lay early groundwork in the field of voice research, specifically, the engineering of voice prostheses to be used in laryngoplasty procedures.

Dystrophic Ossification of Laryngeal Cartilaginous Structures:

During the image segmentation component of this study an interesting incidental finding was noted. It has long been known that as a product of the natural aging process the thyroid, cricoid, and arytenoid cartilages undergo dystrophic endochondral ossification [17]. In the recent past, efforts have been made to document the patterning of ossification in laryngeal cartilages using various imaging methodologies [18]. However, as of yet the 3D structure of laryngeal cartilage ossification patterning has not yet been shown. During the segmentation process we

discovered that we could easily differentiate between cartilaginous and ossified portions of the laryngeal cartilages within our high-resolution MR Images. In all our models we used separate label fields to indicate ossification patterns. Figures 4.9 and 4.10 show the 3D aspects of the patterning of ossification on two larynx specimens. Laryngeal cartilage officiation pattern mapping can be useful in several ways such as, identifying osteosarcoma, needle guidance, and phonatory evaluation in the aging patient.

Structure by MRI Contrast	Tissues and Cell Types
Thyroid, Cricoid, and Arytenoid Cartilage	hyaline cartilage, dystrophic bone
Vocal Fold Mucosa	epithelial, muscular, and glandular tissue comprised of collagen, elastin, ciliated columnar stratified epithelium, sub-mucosal respiratory glands, skeletal muscle, perimysium fascial spaces, loose fibrous connective tissue, and chronic inflammatory cells within the lamina propria
Vestibular Space	N/A
Muscle	skeletal muscle, perimysium, collagen, elastin
Fascia	Perimysium, loose fibrous connective tissue

Figure 4.1 A Table that Lists Several Laryngeal Tissues and Cell Types which were identified via Image Contrast and Histological Analysis. Laryngeal structures identified via MR image contrast and their corresponding tissue types as seen on histological analysis
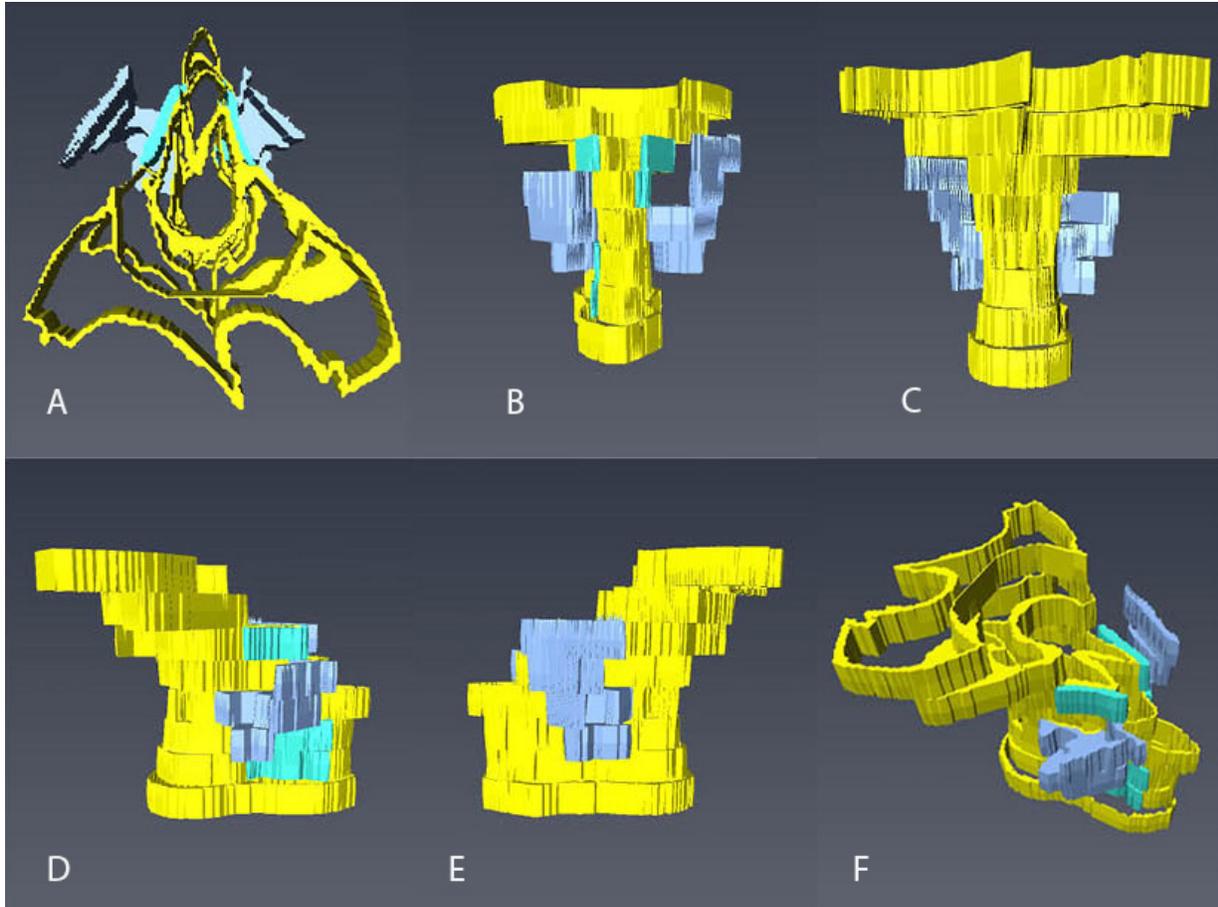
Figure 4.2: The 3D Internal Structures of Human Larynx Specimen 1 are Modeled from Several Aspects. The yellow indicates the central structure of the vocal fold mucosa within the larynx. The darker blue shows the shape of the vestibular opening between the true and false vocal folds while the lighter blue indicates the position of the vocal ligament. Panels A-F depict superior, anterior, posterior, right, left, and best views of the internal laryngeal structures respectively. In panels B-F the top of each panel contains the superior portion of the larynx while the bottom of each panel contains the inferior portion.
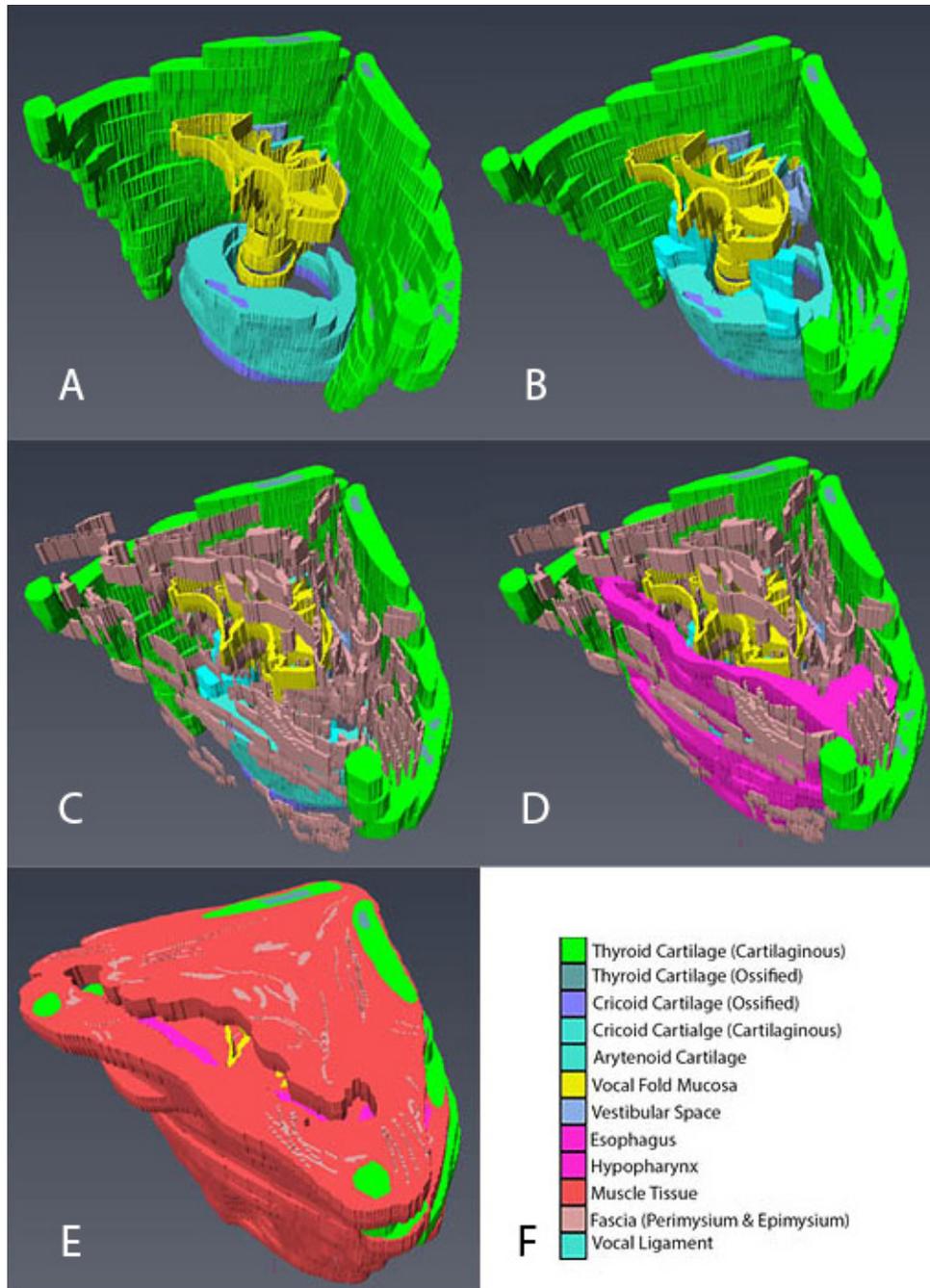
Figure 4.3: Each Panel Displays a 3D Model Depicting the Arrangement of Both the Internal and External Structures of Human Larynx Specimen 1 from a Best View Angled Orientation as Individual Laryngeal Structures are Added. Panel A depicts the cricoid cartilage, thyroid cartilage, vocal fold mucosa, vestibular space, and vocal ligament. Panel B shows the same structures as seen in panel A with the addition of the arytenoid cartilage. Panel C adds fascia visible between musculature on high-resolution MRI. Panel D adds esophageal structure to the model. Finally, intrinsic laryngeal muscles are shown in panel E.
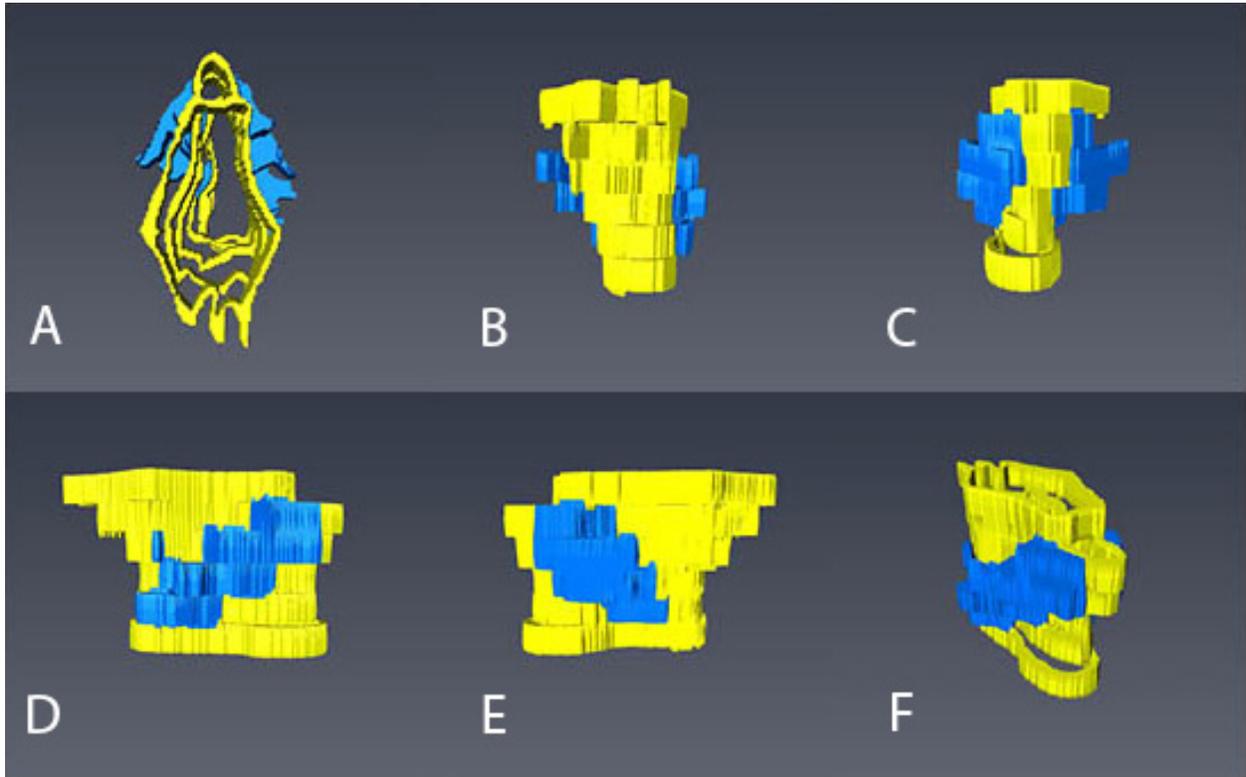
Figure 4.4: The 3D Internal Structures of Human Larynx Specimen 2 are Modeled from Several Aspects. The yellow indicates the central structure of the vocal fold mucosa within the larynx. The blue shows the shape of the vestibular opening between the true and false vocal. Panels A-F depict superior, anterior, posterior, right, left, and best views of the internal laryngeal structures respectively. In panels B-F the top of each panel contains the superior portion of the larynx while the bottom of each panel contains the inferior portion.
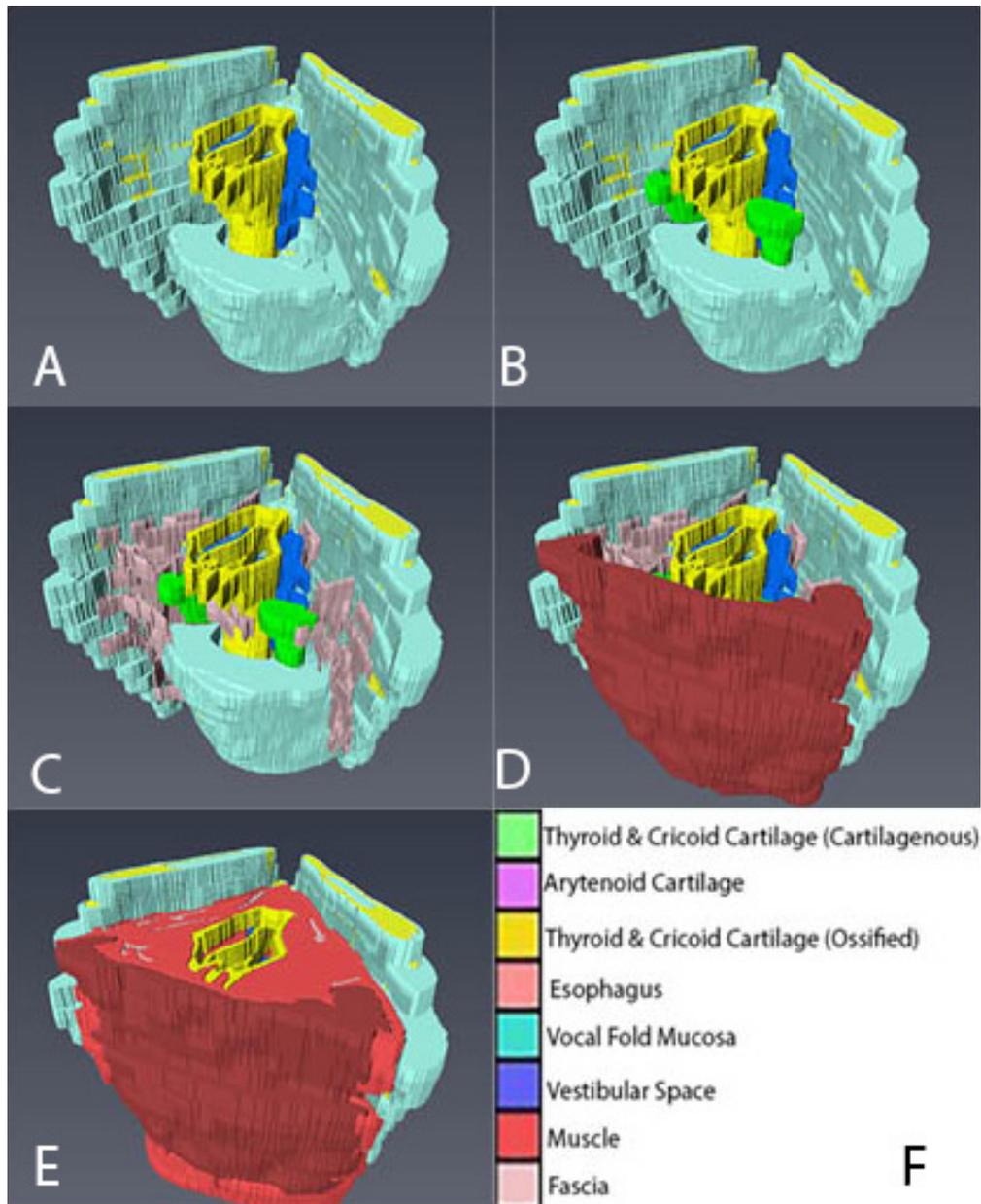
Figure 4.5: Each Panel Displays a 3D Model Depicting the Arrangement of Both the Internal and External Structures of Human Larynx Specimen 2 from a Best View Angled Orientation as Individual Laryngeal Structures are Added. Panel A depicts the cricoid cartilage, thyroid cartilage, vocal fold mucosa, and vestibular space. Panel B shows the same structures as seen in panel A with the addition of the arytenoid cartilage shown in green. Panel C adds fascia visible between musculature on high-resolution MRI. Panel D adds esophageal structure to the model. Finally, intrinsic laryngeal muscles are shown in panel E.
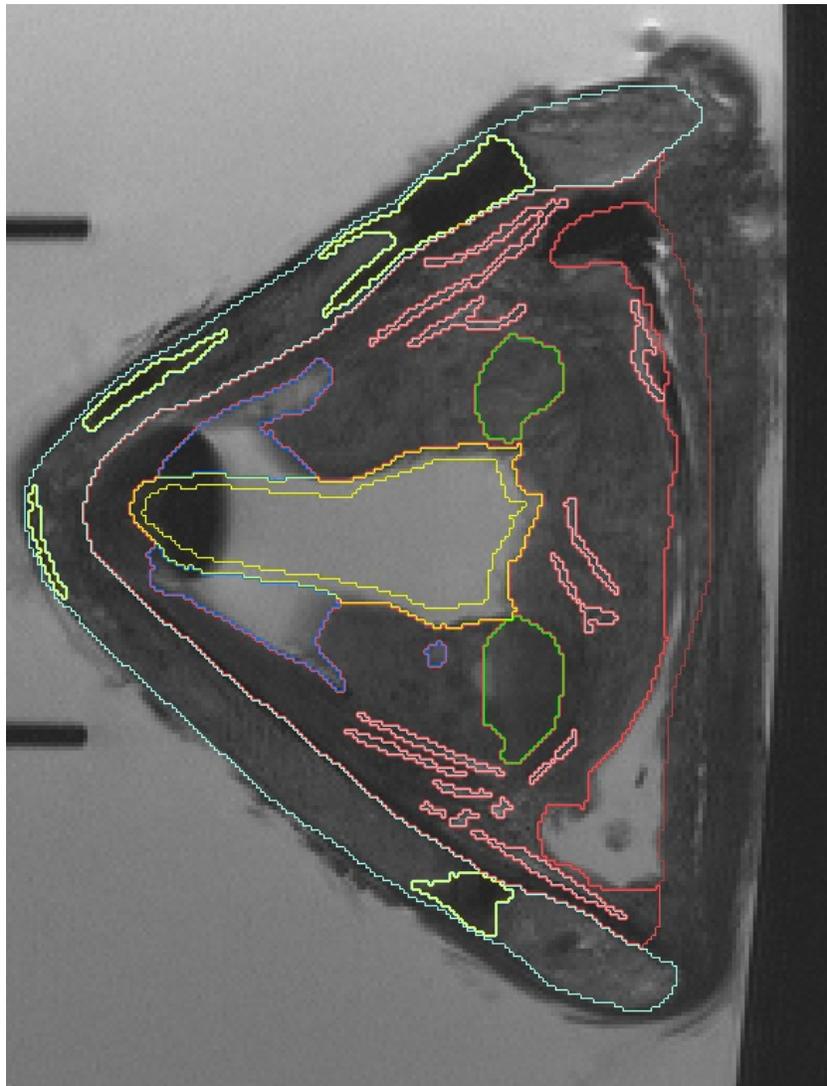
Figure 4.6: A High-Resolution MR Image Slice through a Human Larynx at the Level of the Laryngeal Prominence. Individual tissues and structures are identified by image contrast and carefully segmented and labeled in different colors. Color labels from these segmented image slices are then used to generate 3D models of laryngeal structure with tissue specificity.

Figure 4.7: A Series of Segmented High-Resolution MR Image Slices through a Single Human Larynx Specimen. Panels A-L run from the most inferior slice to the most superior. Individual tissues and structures are identified by image contrast and carefully segmented and labeled in different colors. Color labels from these segmented image slices are then used to generate 3D models of laryngeal structure with tissue specificity.
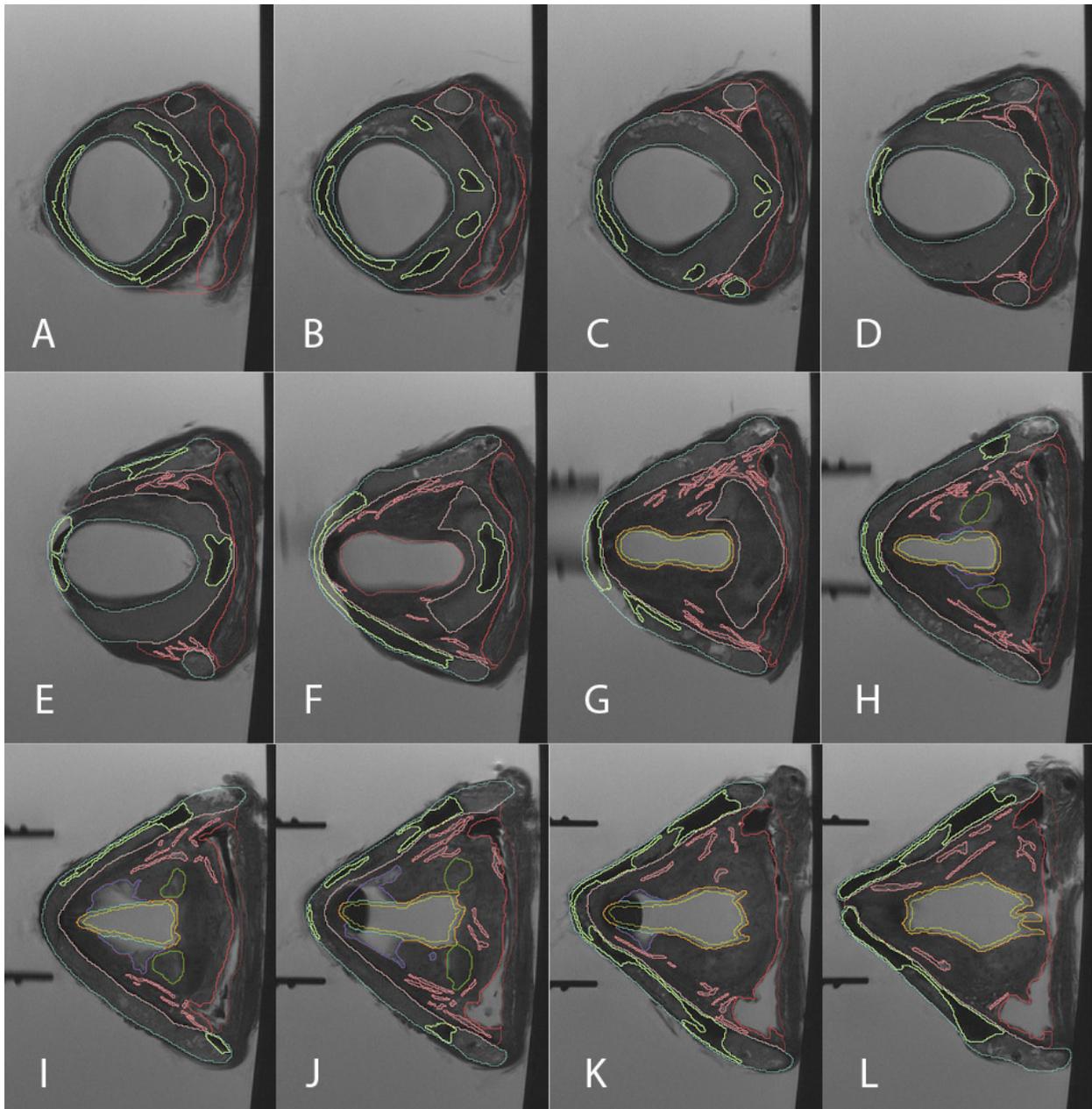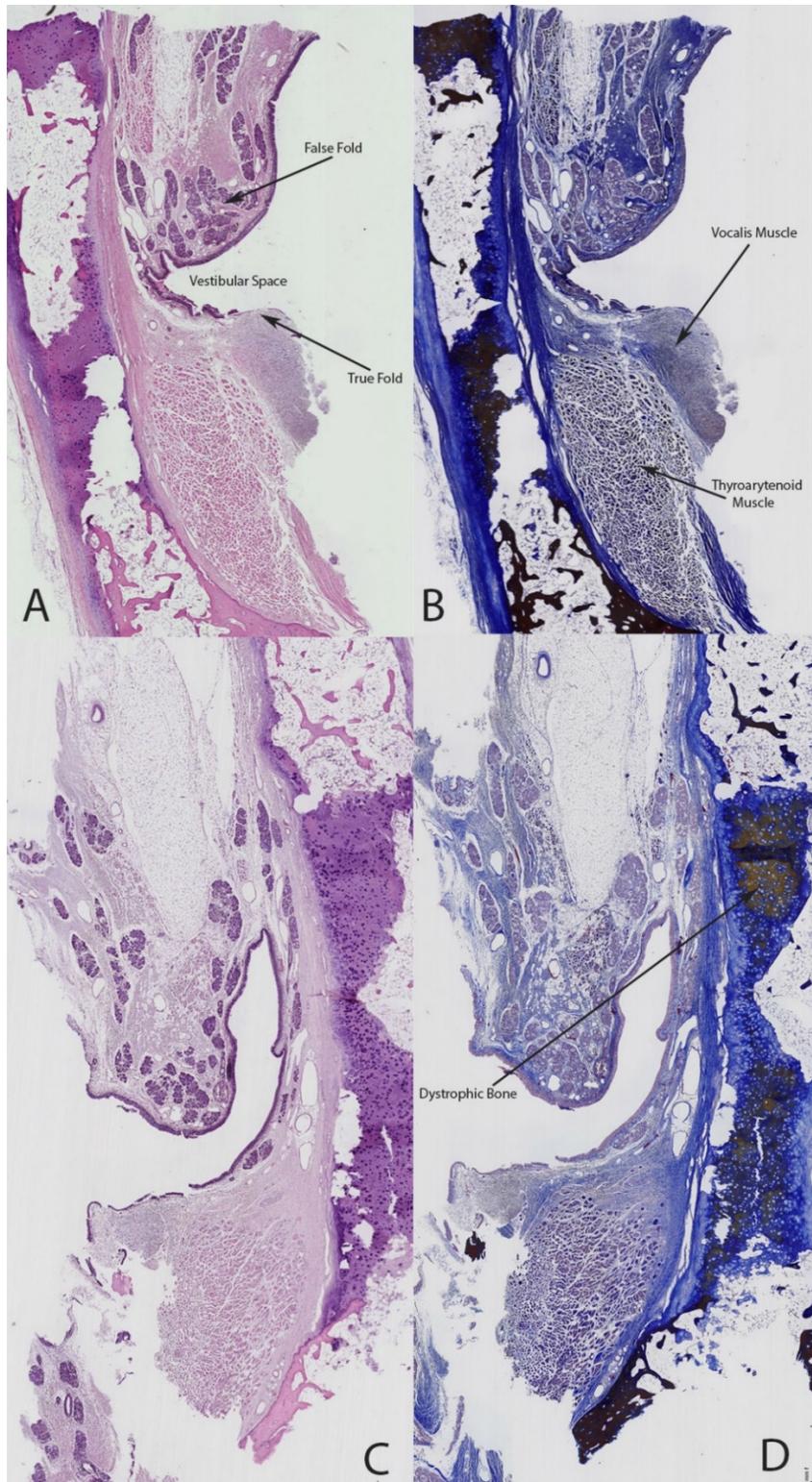
Figure 4.8: Histological analysis of Right and Left halves of the posterior larynx Sliced in the Coronal Plane. Panels A and B show the left side of the larynx, panels C and D depict the right side. Slides shown in panels A and C are H&E stains and panels B and D are Mallory's Trichrome. Tissues of the true and false folds are easily seen in these images.

Figure 4.9: A 3D Model Depicting the Pattern of Ossification within the Cricoid, Arytenoid and Thyroid Cartilage within Human Larynx Specimen 1. Panel A shows the internal 3D pattern of ossification in the thyroid cartilage of human larynx specimen 1 in dark green. Panel B depicts the cartilaginous portions of the thyroid cartilage covering the ossification centers in light green. Panels C and D show ossification of the cricoid cartilage in purple and cartilaginous portions in light blue.
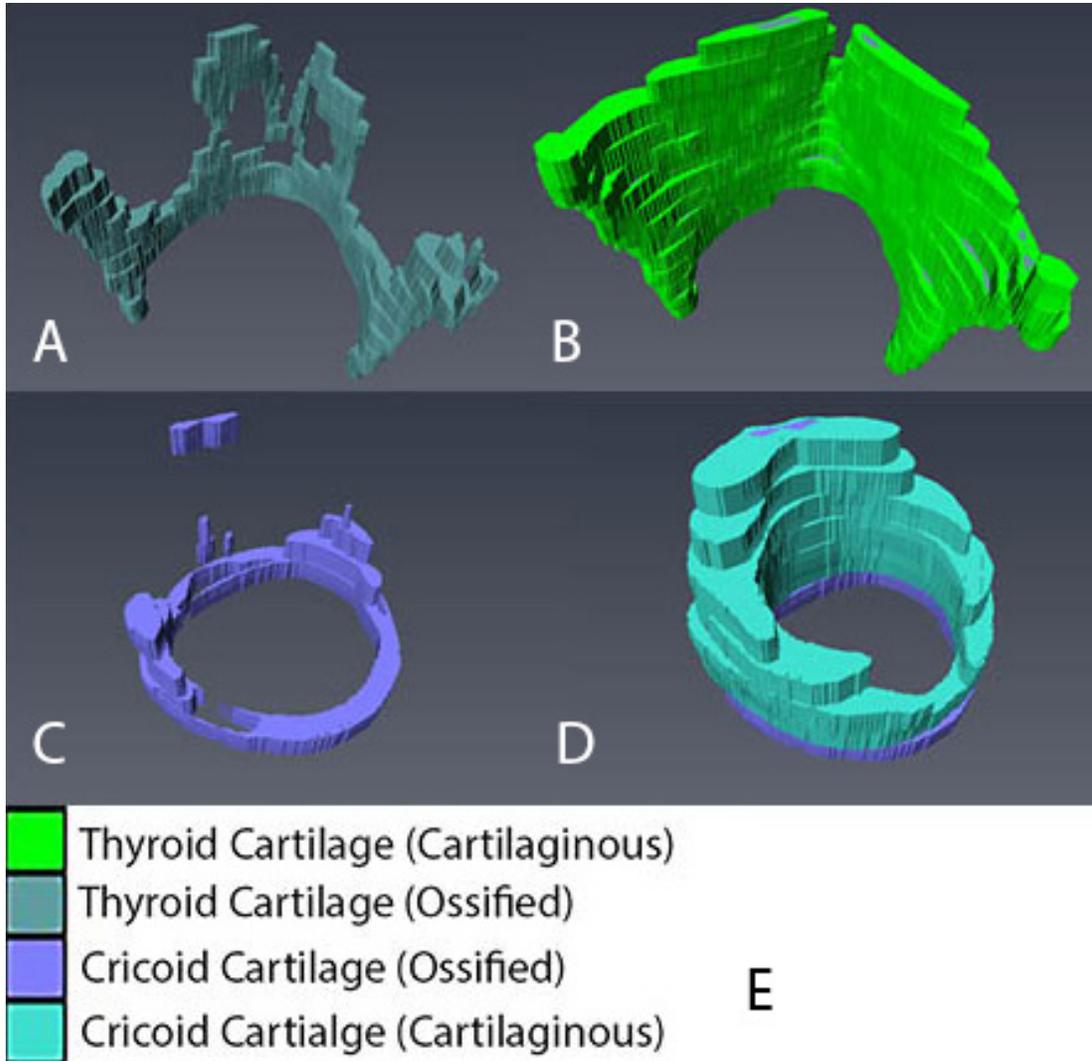
Figure 4.10: A 3D Model Depicting the Pattern of Ossification within the Cricoid, Arytenoid and Thyroid Cartilage within Human Larynx Specimen 3. Panel A shows the internal 3D pattern of ossification in the thyroid cartilage of human larynx specimen 1 in dark green. Panel B depicts the cartilaginous portions of the thyroid cartilage covering the ossification centers in light green. Panels C and D show ossification of the cricoid cartilage in purple and cartilaginous portions in light blue.
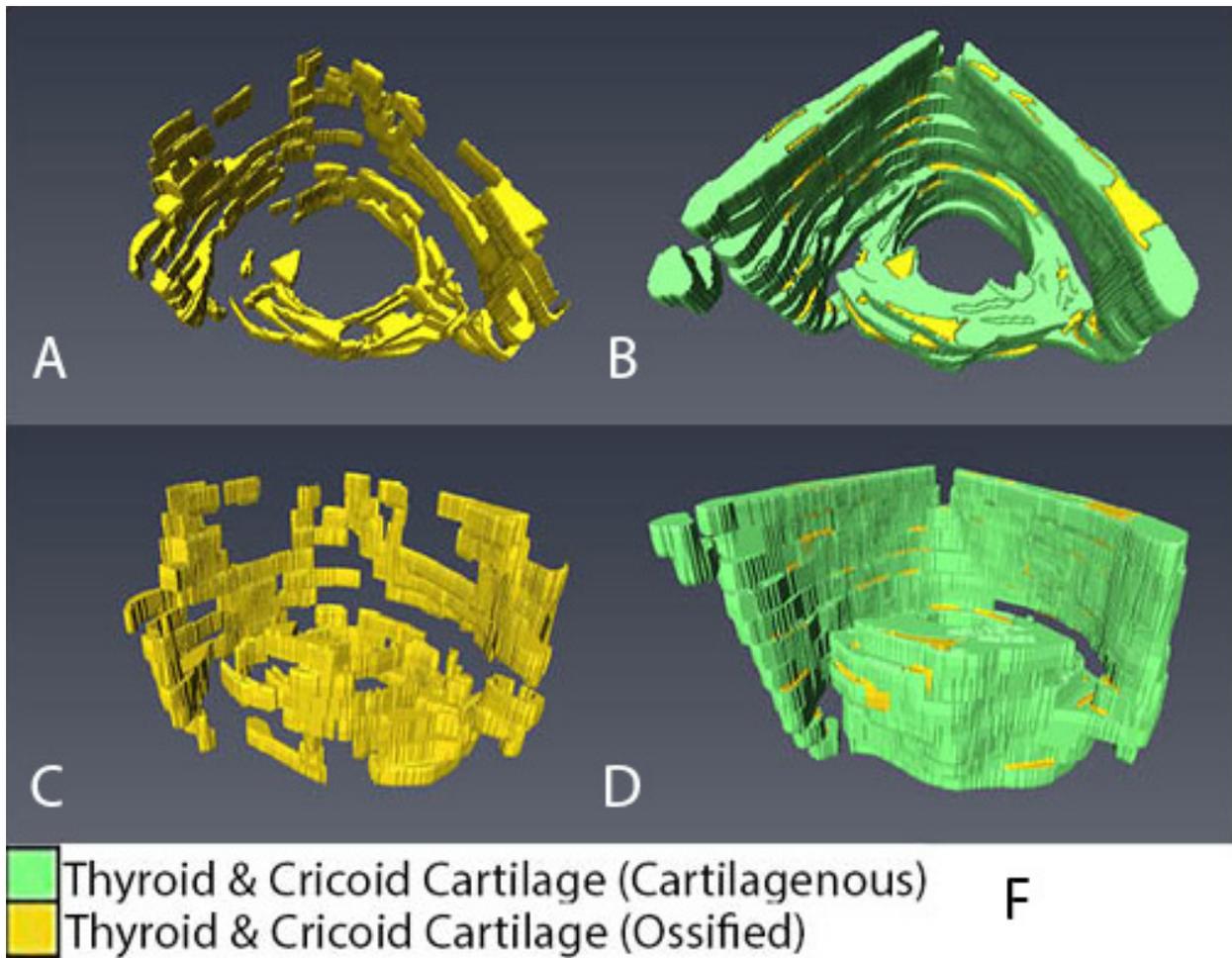
References

1. Ford CN: Advances and refinements in phonosurgery. The laryngoscope 1999, 109(12):1891-1900.

2. Berke GS, Moore DM, Hanson DG, Hantke DR, Gerratt BR, Burstein F: Laryngeal modeling: theoretical, in vitro, in vivo. The Laryngoscope 1987, 97(7):871-881.

3. Alipour F, Berry DA, Titze IR: A finite-element model of vocal-fold vibration. The Journal of the Acoustical Society of America 2000, 108(6):3003-3012.

4. De Vries M, Schutte H, Veldman A, Verkerke G: Glottal flow through a two-mass model: comparison of Navier–Stokes solutions with simplified models. The Journal of the Acoustical Society of America 2002, 111(4):1847-1853.

5. Jiang JJ, Diaz CE, Hanson DG: Finite element modeling of vocal fold vibration in normal phonation and hyperfunctional dysphonia: implications for the pathogenesis of vocal nodules. Annals of Otology, Rhinology & Laryngology 1998, 107(7):603-610.

6. Lous N, Hofmans G, Veldhuis R, Hirschberg A: A symmetrical two-mass vocal-fold model coupled to vocal tract and trachea, with application to prosthesis design. Acta Acustica united with Acustica 1998, 84(6):1135-1150.

7. Tayama N, Kaga K, Chan RW, Titze IR: Geometric characterization of the laryngeal cartilage framework for the purpose of biomechanical modeling. Annals of Otology, Rhinology & Laryngology 2001, 110(12):1154-1161.

8. Spencer M, Siegmund T, Mongeau L: Determination of superior surface strains and stresses, and vocal fold contact pressure in a synthetic larynx model using digital image correlation. The Journal of the Acoustical Society of America 2008, 123(2):1089-1103.

9. Murray PR, Thomson SL: Synthetic, multi-layer, self-oscillating vocal fold model fabrication. Journal of visualized experiments: JoVE 2010(58).

10. Murray PR, Thomson SL: Vibratory responses of synthetic, self-oscillating vocal fold models. The Journal of the Acoustical Society of America 2012, 132(5):3428-3438.

11. Tran QT, Gerratt BR, Berke GS, Kreiman J: Measurement of Young's modulus in the in vivo human vocal folds. Annals of Otology, Rhinology & Laryngology 1993, 102(8):584-591.

12. Hunter EJ, Titze IR: Refinements in modeling the passive properties of laryngeal soft tissue. Journal of Applied Physiology 2007, 103(1):206-219.

13. Alipour-Haghighi F, Titze IR: Elastic models of vocal fold tissues. The Journal of the Acoustical Society of America 1991, 90(3):1326-1331.

14. Chan RW, Titze IR: Viscoelastic shear properties of human vocal fold mucosa: measurement methodology and empirical results. The Journal of the Acoustical Society of America 1999, 106(4):2008-2021.

15. Min YB, Titze IR, Alipour-Haghighi F: Stress-strain response of the human vocal ligament. Annals of Otology, Rhinology & Laryngology 1995, 104(7):563-569.

16. Perlman AL, Titze IR: Development of an in vitro technique for measuring elastic properties of vocal fold tissue. Journal of Speech, Language, and Hearing Research 1988, 31(2):288-298.

17. Hately W, Evison G, Samuel E: The pattern of ossification in the laryngeal cartilages: a radiological study. The British journal of radiology 1965, 38(452):585-591.

18. Mupparapu M, Vuppalapati A: Ossification of laryngeal cartilages on lateral cephalometric radiographs. The Angle Orthodontist 2005, 75(2):196-201.

CHAPTER 5: General Conclusion and Relevance of Research

Recurrent laryngeal nerve (RLN) palsy is a common post-operative complication of many head and neck surgeries. [1-5] RLN palsy is caused by accidental compression or transection of the RLN during surgery, or as a result of trauma. When patients become afflicted with vocal cord paralysis they are susceptible to a loss of phonation, respiratory compromise, or aspiration.[6]

This project encompasses several translational anatomy studies which serve the purpose of increasing our knowledge of, and capability to work with, both the human and the porcine larynx. In general our goals are to either prevent RLN damage through surgical augmentation or to improve repair strategies if any damage that does occur. Several new high-resolution magnetic resonance imaging protocols were developed during these projects that can be utilized to generate high quality images of minute structures in both human and porcine larynges. The Porcine larynx was selected for inclusion is several of these projects due to its similarity to the human larynx [7], and its great potential to serve as a model to improve human laryngeal surgical repairs [8, 9]. Several segmentation techniques were also developed that can be used to render state of the art 3D models of laryngeal anatomy and neuroanatomy. Additionally, tissue processing, sectioning, and staining (H&E and Mallory's Trichrome) techniques were optimized and perfected for use in human and porcine laryngeal tissue. All of these new or optimized methodologies will be useful to the scientific community for future studies that utilize human or porcine laryngeal tissue.

Generally speaking this body of work serves the purpose of shortening 3 gaps in our current knowledge of, and capability to successfully work with, porcine and human laryngeal anatomy. The first gap, which is addressed by chapter 2 of this work, is a lack of modern three-

dimensional mapping of the RLN which highlights anatomical variation. Accurate mapping is essential to good surgical planning. Chapter 2 details the generation and utilization of state of the art 3D modeling of porcine anatomy and neuroanatomy. Those models will make the porcine larynx a much more accessible model to use to improve human laryngeal surgical repairs and interventions.

The second gap this project addresses is the fact that there is a great need for a diagnostic imaging method that can be used to determine which anatomical variation of the RLN is present in a particular patient without exploratory surgery. Unfortunately, many patients with vocal cord paralysis undergo exploratory surgery to determine if they are candidates for a PCA reinnervation procedure only to discover they don't have the indicated RLN anatomy for surgical anastomosis. Chapter 3 of this work provides new MRI and segmentation strategies that can be used to reconstructed laryngeal neurovascular structure in 3 dimensions in a noninvasive manner.

The third and final gap addressed by chapter 4 is the determination of the 3D histological geometric structure of the human larynx. We have presented H&E and Mallory's Trichrome histological analysis of human laryngeal tissue alongside complete 3D models of laryngeal structures. A simple correlatory method is suggested to easily extrapolate the 3D histologic geometry of laryngeal structure by analyzing our models alongside histological slides. We intend this information to be useful to those groups seeking to build functional synthetic models of the human vocal apparatus.

 In conclusion we hope that these new methodologies and models will serve the scientific and clinical communities in improving the success of laryngeal surgical repair techniques via improved preclinical studies that use the porcine model, augmented surgical planning, and more realistic synthetic models of laryngeal anatomy and physiology.

References

1. Chiang F-Y, Wang L-F, Huang Y-F, Lee K-W, Kuo W-R: Recurrent laryngeal nerve palsy after thyroidectomy with routine identification of the recurrent laryngeal nerve. Surgery 2005, 137(3):342-347.

2. Crumley R: Phrenic nerve graft for bilateral vocal cord paralysis. The Laryngoscope 1983, 93(4):425-428.

3. Crumley R: Laryngeal synkinesis: its significance to the laryngologist. The Annals of otology, rhinology, and laryngology 1989, 98(2):87-92.

4. Jatzko GR, Lisborg PH, Müller M, Wette VM: Recurrent nerve palsy after thyroid operations--principal nerve identification and a literature review. Surgery 1994, 115(2):139-144.

5. Kwak PE, Friedman AD, Lamarre ED, Lorenz RR: Selective reinnervation of the posterior cricoarytenoid and interarytenoid muscles: an anatomical study. The Laryngoscope 2010, 120(3):463-467.

6. Mårtensson H, Terins J: Recurrent laryngeal nerve palsy in thyroid gland surgery related to operations and nerves at risk. Archives of surgery 1985, 120(4):475-477.

7. Jiang JJ, Raviv JR, Hanson DG: Comparison of the phonation-related structures among pig, dog, white-tailed deer, and human larynges. ANNALS OF OTOLOGY RHINOLOGY AND LARYNGOLOGY 2001, 110(12):1120-1125.

8. Gorti GK, Birchall MA, Haverson K, Macchiarini P, Bailey M: A preclinical model for laryngeal transplantation: anatomy and mucosal immunology of the porcine larynx. Transplantation 1999, 68(11):1638-1642.

9. Knight MJ, McDonald SE, Birchall MA: Intrinsic muscles and distribution of the recurrent laryngeal nerve in the pig larynx. Eur Arch Otorhinolaryngol 2005, 262(4):281-285.

CURRICULUM VITAE

NENA LUNDREEN MASON

5631 Foxview Way, Elk Gove CA 95757. 208-249-0558. nenalundgreen@gmail.com

Education

Doctor of Philosophy; Physiology and Developmental Biology. Brigham Young University (IP)
2015

- (Dissertation: *The Anatomy of Porcine and Human Larynges: Structural Analysis and High Resolution Magnetic Resonance Imaging of the Recurrent Laryngeal Nerve*)

Bachelor of Science; Human Biology. Brigham Young University-Idaho
2012

Teaching Experience (Chronological)

Teaching Assistant: Anatomy and Physiology I. Brigham Young University-Idaho
2009-2012

- Prepared and delivered traditional lectures, served students in the class by providing large group, small group, and individual tutoring, mentored students with special needs through individual tutoring, taught anatomy laboratory courses

Teaching Assistant: Anatomy and Physiology II. Brigham Young University-Idaho
2010-2012

- Prepared and delivered traditional lectures, served students in the class by providing large group, small group, and individual tutoring, mentored students with special needs through individual tutoring, taught anatomy laboratory courses

Academic Support: Physiology, Anatomy, Pathophysiology Salt Lake Community College
2012

- Provided large group sessions of finals reviews for anatomy classes and physiology classes, one on one tutoring

Teaching Assistant: Advanced Physiology. Brigham Young University
2012-2013

- Prepared and delivered several lectures, ran finals reviews, one on one tutoring, became skilled at exam design and exam question generation, graded assignments

Instructor: Advanced Physiology Laboratory. Brigham Young University
2012-2014

- Taught the advanced physiology laboratory class, delivered traditional lectures, grading, exam preparation, experimental equipment set up and operation

Instructor: Gross Anatomy. The University of Utah School of Medicine
2014

- Taught gross anatomy laboratory and dissection techniques

Instructor of Anatomy and Physiology: California Northstate University
College of Medicine
2015-Present

- Designed and delivered full load of physiology lectures to first and second year medical students. Designed interactive physiology curricula that makes heavy use of drawing including both traditional lecture and flipped classroom style lecture strategies. Instructed students in gross anatomy laboratory sessions preformed prosection for student use.

Clinical Experience

Medical Assistant: Kenai Medicenter, (Kenai AK)

- Gained clinical proficiency as an EKG technician, ultrasound technician, X-ray technician and as a medical scribe. Acquired skills in phlebectomy, phlebotomy, and trauma care

Research Experience

Research Assistant: Dr. David Busath Laboratory. Physiology and Developmental Biology Department. Brigham Young University 2012.

- Preformed electrophysiology of viral proton pumps. Xenopus oocyte RNA expression.

Research Assistant: Dr. Jeffery Edwards Laboratory. Physiology and Developmental Biology Department. Brigham Young University 2013.

- Implemented protocols for patch clamping while studying synaptic plasticity in the VTA and hippocampus

Research Assistant: Dr. Wisco's Laboratory for Translational Anatomy of Degenerative Diseases and Developmental Disorders. Physiology and Developmental Biology Department. Brigham Young University 2014.

- Acquired high resolution structural MR images. Preformed MR image segmentation in Amira (FEI) and generated of 3D anatomical models with Maya molding software (Autodesk). Used MicroScribe digitization to create state of the art anatomical mapping. Preformed professional dissection of larynges and whole cadavers. Histological staining (H&E and Mallory's trichrome)

Peer-Reviewed Publications & Abstracts

In Print:

3D Reconstruction and Heat Map of Porcine Recurrent Laryngeal Nerve Anatomy: Branching and Spatial Location, Nena Lundgreen Mason; Marc Christiansen; Jonathan J. Wisco Ph.D., Italian Journal of Anatomy and Embryology, vol. 120, 2015; Department of Physiology and Developmental Biology, Brigham Young University, Provo, UT

In Review:

Use of High-Resolution Magnetic Resonance Imaging to Reconstruct Recurrent Laryngeal Nerve Structure in 3D, Nena Lundgreen Mason, Scott Robison, Jonathan J. Wisco Ph.D., Department of Physiology and Developmental Biology, Brigham Young University, Provo, UT (in progress)

Modeling of the 3D geometric structure and tissue composition of human laryngeal anatomy via high-resolution MRI segmentation and histological analysis, Nena Lundgreen Mason[1], Haonan Wang[2], Brett Heldt[1], BreAnna Long[1], ReyLynn Reid[1], Amin Nazaran[2], Brett Gardiner[1], Neal K. Bangerter Ph.D.[2], Jonathan J. Wisco Ph.D.[1,3], [1]Department of Physiology and Developmental Biology, Neuroscience Center, Brigham Young University, Provo UT, [2]Department of Electrical and Computer Engineering, Brigham Young University, Provo UT, [3]Department of Neurobiology and Anatomy, University of Utah School of Medicine, Salt Lake City, UT (in progress)

Meeting Abstracts:

Use of High-Resolution Magnetic Resonance Imaging to Reconstruct Recurrent Laryngeal Nerve Structure in 3D, American Association of Anatomists EB Boston 2015

3D Rendering of Porcine Recurrent Laryngeal Neuroanatomy, American Association of Anatomists EB Boston 2015

Professional Memberships

American Association of Clinical Anatomists. Member, 2013-Present

Society for Neuroscience Intermountain Branch: Brigham Young University. Member 2012-Present

American Association of Anatomists. Member, 2013-Present

International Association of Medical Science Educators 2015- Present

Community Service

Docent: Museum of Idaho, Idaho Falls, ID, Bodies the Exhibition

Relief Society Presidency: The Church of Jesus Christ of Latter-Day Saints

2010-2012

Freshman Orientation Mentor: Brigham Young University--Idaho 2009-2011